AD-A033 487 PENNSYLVANIA STATE UNIV UNIVERSITY PARK APPLIED RESE--ETC F/G 20/2
HELIUM ATOMIC BEAM SCATTERING FROM CLEAN (001) SURFACES OF NAF.(U)
OCT 76 M P LIVA N00017-73-C-1418
UNCLASSIFIED TM-76-250 NL

1 OF 1
AD
A033487

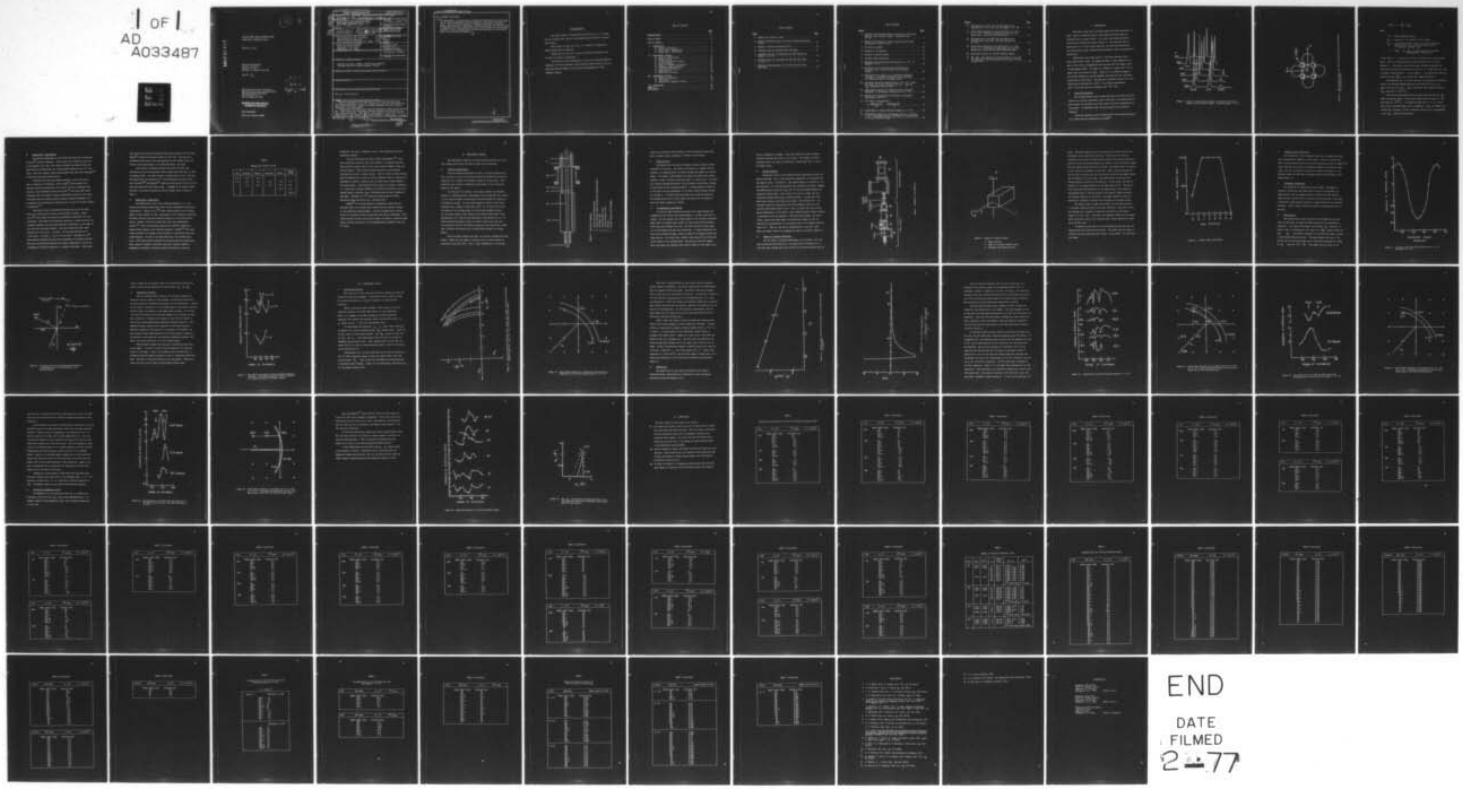

END

DATE
FILMED
2-77

12

HELIUM ATOMIC BEAM SCATTERING FROM CLEAN (001) SURFACES OF NaF*

Michael P. Liva

Technical Memorandum
File No. TM 76-250
October 5, 1976
Contract No. N00017=73=C=1418

Copy No. 6

The Pennsylvania State University
Institute for Science and Engineering
APPLIED RESEARCH LABORATORY
Post Office Box 30
State College, PA 16801

NAVY DEPARTMENT

NAVAL SEA SYSTEMS COMMAND

UNCLASSIFIED
SECURITY CLASSIFICATION OF THIS PAGE (When Data Entered)

REPORT DOCUMENTATION PAGE	READ INSTRUCTIONS BEFORE COMPLETING FORM
(14) REPORT NUMBER: TM-76-250 (9) Technical memo.	2. GOVT ACCESSION NO. / 3. RECIPIENT'S CATALOG NUMBER
4. TITLE (and Subtitle): (6) HELIUM ATOMIC BEAM SCATTERING FROM CLEAN (001) SURFACES OF NaF	5. TYPE OF REPORT & PERIOD COVERED: M.S. Thesis, November 1976
	6. PERFORMING ORG. REPORT NUMBER: TM 76-250
7. AUTHOR(s): (10) Michael P. Liva (11) 5 Oct 76	8. CONTRACT OR GRANT NUMBER(s): (15) N00017-73-C-1418
9. PERFORMING ORGANIZATION NAME AND ADDRESS: The Pennsylvania State University, Applied Research Laboratory, P. O. Box 30, State College, PA 16801	10. PROGRAM ELEMENT, PROJECT, TASK AREA & WORK UNIT NUMBERS: (12) 78 p.
11. CONTROLLING OFFICE NAME AND ADDRESS: Naval Sea Systems Command, Department of the Navy, Washington, D.C. 20362	12. REPORT DATE: October 5, 1976
	13. NUMBER OF PAGES: 76 pages & figures
14. MONITORING AGENCY NAME & ADDRESS (if different from Controlling Office)	15. SECURITY CLASS. (of this report): Unclassified, Unlimited
	15a. DECLASSIFICATION/DOWNGRADING SCHEDULE

16. DISTRIBUTION STATEMENT (of this Report)

Approved for public release, distribution unlimited, per NSSC (Naval Sea Systems Command), 10/18/76

17. DISTRIBUTION STATEMENT (of the abstract entered in Block 20, if different from Report)

18. SUPPLEMENTARY NOTES

19. KEY WORDS (Continue on reverse side if necessary and identify by block number)

Molecular beam Scattering

20. ABSTRACT (Continue on reverse side if necessary and identify by block number)

Several improvements were developed for the atomic beam apparatus, including stabilization of the inlet temperature, cooling of the sample and the titanium sublimator, methods of precise alignment, and more accurate measurement of the beam angles.

Measurements were made on the selective adsorption energy levels of He on NaF. Three levels were determined with good accuracy and a fourth one was also roughly determined. From these, a well depth of 7.5 meV and a Van der Waals constant, C_3 = 140 meV - A^2, can be estimated. → next page

DD FORM 1 JAN 73 1473 EDITION OF 1 NOV 65 IS OBSOLETE

C(3) A squared

UNCLASSIFIED
SECURITY CLASSIFICATION OF THIS PAGE (When Data Entered)

391007

7/8

20. ABSTRACT (Continued)

cont

Measurements of intensities of diffracted beams were also carried out, and the two new phenomena recently predicted on theoretical grounds were found. These are the occurrence of intensity maxima due to multiple transitions (incident to adsorbed to diffracted states), and the splitting of degeneracies in the energy levels due to perturbations by the periodic potential. Both of these effects provide new approaches to the determination of the potential parameters.

A

ACKNOWLEDGMENTS

The author wishes to express his gratitude to Dr. D. R. Frankl for his constant help, advice, and enlightening discussions throughout this project.

Many thanks are also due to Dr. J. A. Meyers for helping the author understand the apparatus.

Thanks are also due to W. Carlos for helpful discussions, and G. Derry for technical assistance.

The National Science Foundation, as well as the Applied Research Laboratory of The Pennsylvania State University under contract with the Naval Sea Systems Command, are gratefully acknowledged for their financial support.

TABLE OF CONTENTS

LIST OF TABLES

LIST OF FIGURES

I. INTRODUCTION

This report deals with a molecular beam scattering experiment, in which a beam of molecules having a known energy (and wavelength) is scattered from a crystal surface. As in most scattering experiments, reflection and diffraction result (Figure 1). The molecular beam is used because it is very surface sensitive, the molecules interacting only with surface atoms, thereby giving information about the gas-surface interaction.

Specifically the system used is a ^{4}He beam scattering from a clean (001) plane of NaF. The sample was kept at room temperature for most of this study, although some work was done with the sample cooled to approximately 80°K. The sample is cleaved in a vacuum $<10^{-9}$ torr to assure that the surface is clean. Figure 2 is a schematic diagram of the surface showing the crystallographic directions and the coordinate system used in this report. The beam has an incident energy of 17.6 mev which gives a wavelength of 1.08 Å. It is fairly monochromatic ($\Delta\lambda/\lambda \approx 0.02$) and very well collimated ($\Delta\theta < 10^{-3}$ rad).

A. Selective Adsorption

One striking feature seen in molecular beam scattering from ionic crystals is selective adsorption, which occurs when an incoming particle gets trapped in a potential well with respect to motion perpendicular to the surface. It manifests itself as sharp minima in the reflected intensity.

Selective adsorption can be explained with the following equation, which comes from the conservation of energy:[1]

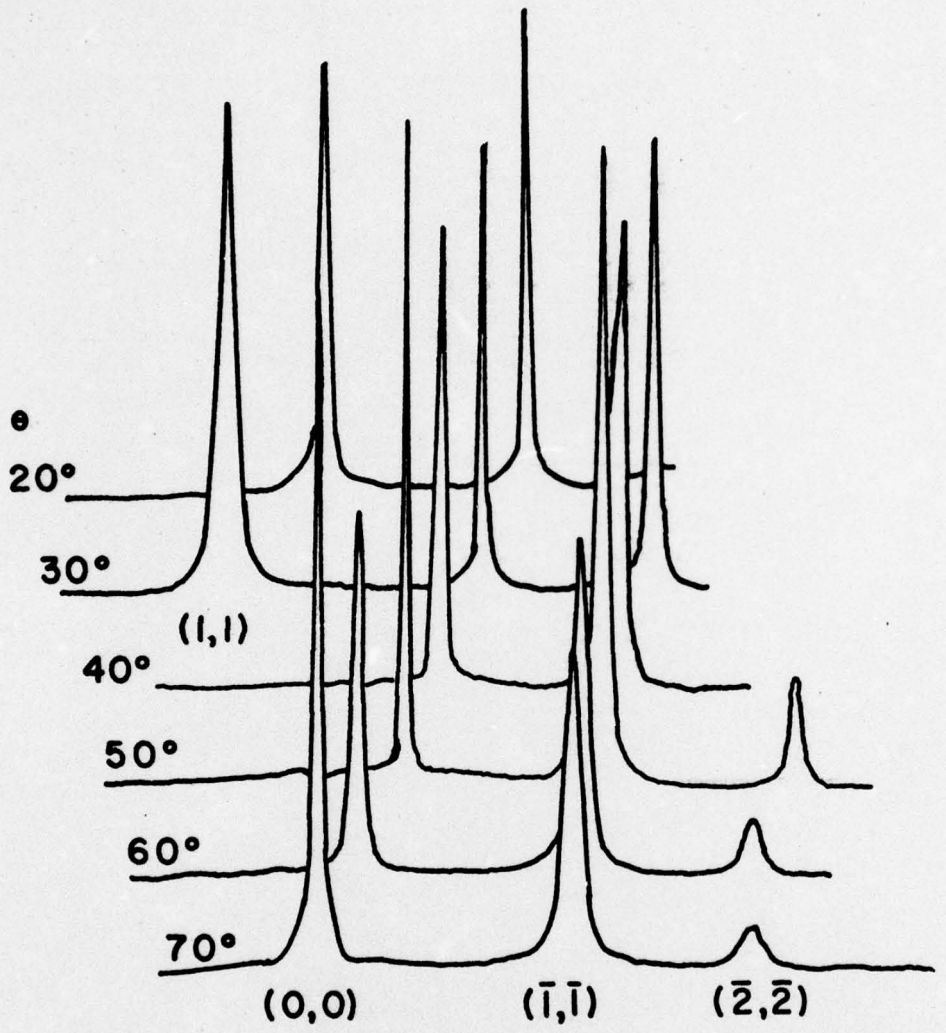

Figure 1. Detector Scans Showing Specular and In-Plane Diffracted Beams at Fixed Incident Angles. Azimuthal Angle $\phi = 45°$.

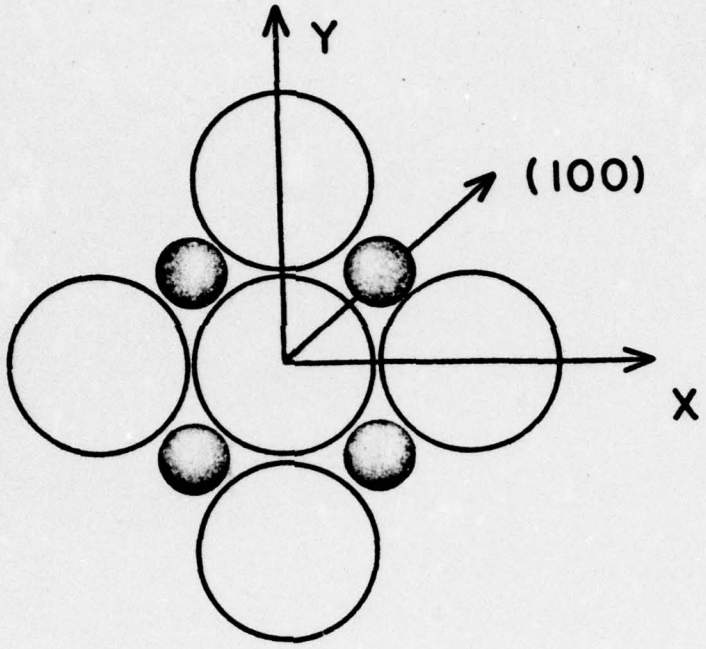

Figure 2. Surface Mesh Showing the [100] Crystal Direction and Defining the Coordinate Axes.

$$|\vec{k}|^2 + \varepsilon = (\vec{K}_{\parallel} + \vec{G}_{mn})^2 \quad , \tag{1}$$

where

$\vec{k}$ = the incident wavevector ,

$\vec{K}_{\parallel}$ = the part of $\vec{k}$ parallel to the surface ,

$\vec{G}_{mn}$ = a reciprocal lattice vector to the (mn) reciprocal lattice point. $\vec{G}_{mn} = 2\pi/a\ (m\hat{x} + n\hat{y})$, where $a = 1.9175$ Å for NaF , and

$\varepsilon = |k_z'|^2$, k_z' being the final wavevector component perpendicular to the surface.

If the value of ε is greater than zero, the particle is in an unbound state. This is a diffracted beam, and is referred to as an "open channel"; ε may take on any positive value allowed by Equation (1). The selective adsorption bound state occurs if ε is less than zero, the so-called "closed channel". In this region, ε can assume only discrete values such that $\frac{\hbar^2}{2m}\varepsilon_n$ is a bound state (negative) energy.

From Equation (1), it can be seen that if the selective adsorption points, the observed minimum positions, are plotted in the k_x, k_y plane, circles will result. These circles will have centers located at $-\vec{G}_{mn}$ and radii of $\sqrt{k^2 + \varepsilon_n}$.

The selective adsorption points can also be plotted in the $\vec{G}_{mn}$ plane (reciprocal space). Circles will again result centered at $-\vec{K}_{\parallel}$ with radii of $\sqrt{k^2 + \varepsilon_n}$. It should be noted that if $\varepsilon = 0$, such a plot is just the Ewald sphere in two dimensions. Also, the energy level circles will intersect the (mn) reciprocal lattice point, corresponding to the $\vec{G}_{mn}$ transition taking place.

B. Recent Work: Experimental

The earliest experiments in this field were done over 45 years ago by Stern[2] and his co-workers. Their results were limited by the state of technology at the time, most notably effusion beam sources which had wide velocity distributions, and vacuum systems working in the 10^{-5} torr range. They did, however, observe some minima which were later explained[3] as selective adsorption bound states.

Currently, there has been renewed interest in this field due in part to advances in technology. Nozzle beams,[4] which produce much narrower velocity distributions than effusive sources, quadrupole mass filters, narrow bandwidth velocity selectors,[5] and ultra high vacuum techniques have all helped to improve experimental results in this field. At present, there are several groups working on similar experiments (for a review, see the introduction of Reference 6), as well as on other classes of materials.[7]

Most work to date on non-metals has been done on LiF surfaces, with less on NaF and very little on other alkali halides. Finzel et al.[8] have looked at reflected and diffracted intensities of H and D from NaF. They found strong specular reflection, as much as 38% of the incident intensity, but only weak diffracted intensities, on the order of one tenth the reflected intensity. They have identified three bound states for H (-11.8 ± 0.2, -3.0 ± 0.2, -0.4 ± 0.4 mev) and four for D (-11.8 ± 0.2, -5.8 ± 0.2, -1.6 ± 3, 0.3 ± 0.3 mev). Williams et al.[9] have studied reflected and diffracted intensities of He and Ne from NaF. They have used different energies and surface temperatures to study the broadening of diffracted beams due to inelastic collisions. Their work

has yielded two selective adsorption bound state energies for He on NaF. Meyers[6] reported three bound states for He on NaF. His work was a preliminary study done on the same apparatus as the present study, but before certain improvements to be described below were made.

Stern and his co-workers did some work with He on NaF, and although they did no calculations, later workers used their data to find the energy levels. The first attempt to analyze Stern et al's data was by Lennard-Jones and Devonshire.[3] They identified two bound states. Later Tsuchida[10] and Bledsoe[11] again did calculations on Stern et al's data and identified three bound states. A summary of the energy values obtained in the above calculations and the present study is given in Table 1.

C. Recent Work - Theoretical

The minima which occur in the reflected intensity, i.e., the selective adsorption bound states, have stirred considerable theoretical investigation. Cabrera et al.[12] used a Morse potential and a limited number of open channels in their calculation of the scattered intensities. The Morse potential was used primarily because it can be analytically solved. However, it does not agree well with recent experimental results.[1] Their calculations predicted that selective adsorption should produce maxima in the reflected intensity. Wolken[13] also used a Morse potential and extended the calculation to include both open and closed channels. He came to the same conclusion, that maxima should occur. Both these authors explained the observed minima by postulating that a particle trapped in the bound state has a greater chance of undergoing an inelastic collision, which would scatter it into the

TABLE 1

Energy Level Values for NaF

LJD	Tsuchida	Bledsoe	Williams	Meyers	Present Study
8.4	8.3	8.5			
3.5	4.8	4.9	4.8	5.0	4.9
	1.9	2.0	1.8	1.9	1.8
				0.5	0.6
					0.003

background and cause a minimum to occur. This explanation has been generally accepted.

A recent calculation was done by Chow and Thompson.[14] They used a different potential than other workers, a corrugated hard wall with attractive square well in front, and a greater number of open and closed channels. Their results predicted minima in the reflected intensity due purely to elastic events. That is, unlike earlier workers, Chow and Thompson do not have to rely on inelastic events to explain the experimental results. Another result of their work is their multiple scattering theory. They predicted that a particle can make a transition to a bound state, giving a minimum in the reflected intensity, but then undergo another transition into a diffracted beam, giving a maximum in that beam. Williams et al.[9] reported seeing maxima in certain diffraction beams but did not do a detailed study.

LeRoy,[15] in a recent empirical calculation, found that the one-sixth power of the bound state energy value was linearly related to the vibrational quantum number. He also concluded that no unique form of the potential could be found from this type of experiment. What could be found, he said, was the well depth, the number of possible bound states, and the coefficient of the asymptomatically dominant term, the Z^{-3} term.

II. EXPERIMENTAL METHODS

The experimental apparatus has been described earlier (16, 6) so only changes made during the present study will be discussed.

A. Velocity Stabilization

An early problem encountered was that of velocity stabilization. Over the time of a data run the beam velocity and therefore the initial energy was not constant, with changes as much as 2% occurring. These variations were traced to temperature fluctuations of the cooled gas supply at the nozzle.

To alleviate this problem, a new nozzle assembly was designed (Figure 3), embodying several improvements over the previous one, namely, (1) the liquid nitrogen cooling jacket and feed-through are completely surrounded by vacuum, (2) the feed-throughs are made of thin walled stainless steel tubing to reduce heat flow, (3) to reduce heat input by radiation, the cooling jacket is covered with aluminized mylar, (4) the nozzle support which formerly was a snug-fitting brass collar approximately 1/2" long has been machined out and replaced with a .05" thick snug-fitting plastic collar to further reduce heat flow, and (5) the gravity feed of the liquid nitrogen has been replaced by a pump that circulates the liquid from a storage dewar through the cooling jacket.

After the above changes were made, the velocity remained much more stable. Typically, the change in velocity over a six-hour period of operation is now only 0.25%. Also, a lower temperature of the He gas

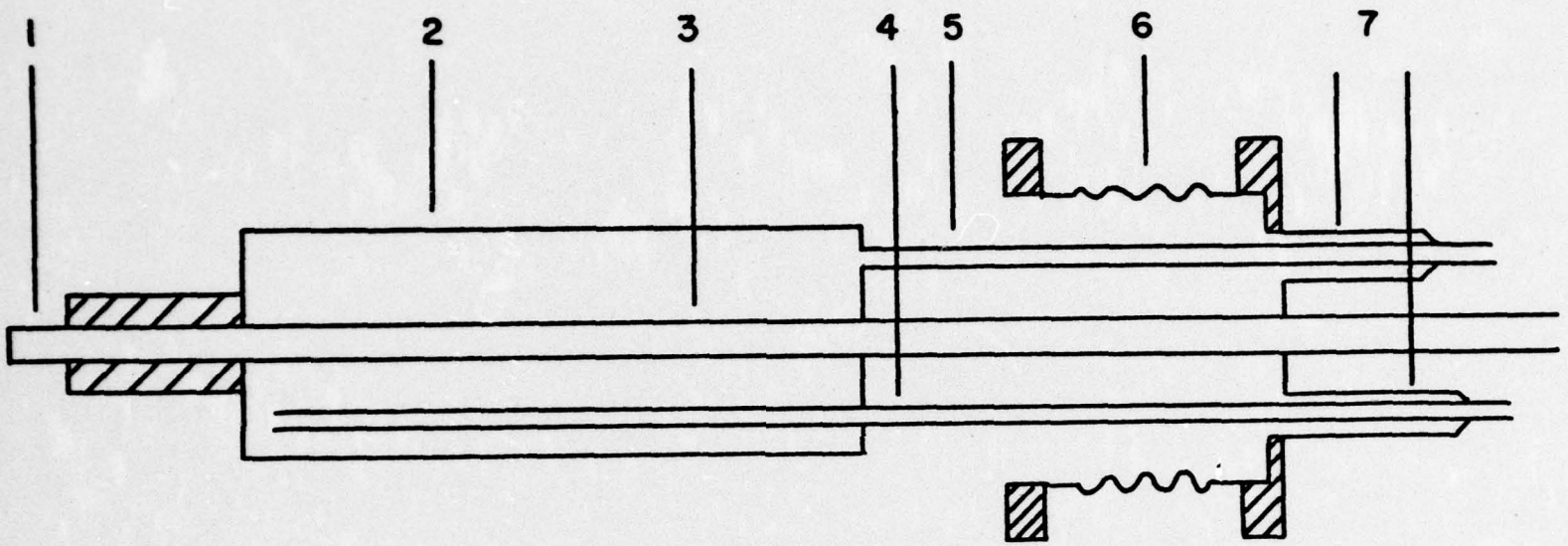

Figure 3. New Nozzle Assembly.

1. Nozzle Cap with Thermocouple.
2. Liquid Nitrogen Jacket Covered with Aluminized Mylar.
3. Gas Inlet Tube.
4. Liquid Nitrogen Inlet.
5. Liquid Nitrogen Outlet.
6. Bellows.
7. Vacuum Jacketed Feed-Throughs.

supply is now possible (78°K compared to 90°K previously) which means that a slightly longer wavelength of 1.08 Å is now obtained.

B. Sample Cooling

Preliminary work was done with sample cooling to reduce thermal vibrations of the atoms. The effect of cooling is to improve surface features, for example, minima are usually sharper and deeper on a cooled sample. The sample is held between two copper jaws which have sliding contacts on them, thermally connecting them to a copper plate. The plate has a liquid nitrogen reservoir on it and flexible cooling lines leading to the bottom of the scattering chamber. A storage dewar is connected to the input line and pressurized to circulate liquid nitrogen through the reservoir. A solenoid valve and timer can be used to pressurize the storage dewar since it takes about three hours for the sample to reach its lowest temperature (≈80°K).

C. Ti Sublimation Pump Cooling

In order to keep residual gas atoms in the vacuum system from condensing on the surface and contaminating it, a large cooled area is needed. For this purpose the cooling jacket of the titanium sublimation pump, which is normally water cooled, is cooled with liquid nitrogen. There were some problems with this. The inlet and outlet water pipes are in the flanges that make the vacuum seal. If these connections are used for the liquid nitrogen, uneven cooling of the flanges results and leaks open up. To correct this, another inlet connection was installed in the center of the cooling jacket, some distance from the flanges. Also, the jacket was insulated with several layers of foam rubber up to,

but not including the flanges. With this system the liquid nitrogen is gravity fed into the center of the jacket. The flanges cool more uniformly and do not leak, and sufficient cooling takes place to keep the sample clean.

D. System Alignment

During the course of this study, the entire apparatus was moved to another building. Due to this moving, the system had to be realigned and the angular scales recalibrated. The system (Figure 4) consists of two main sections: (1) the beam formation part including the nozzle, skimmer, and pinhole which define the beam, and (2) the scattering chamber and associated vacuum pumps. Each section is on its own frame, the only connection between them being a flexible bellows. To make each frame more rigid, several extra braces were added. Fine thread (1/2" - 27) leveling screws were installed on the beam formation section so that accurate positioning could be done. Also, to insure that each section moved independently of the other, a more flexible bellows (bronze instead of stainless steel) was installed. With the above changes, and using levels, squares and light beams, the system was aligned so that the beam axis was perpendicular to the vertical axis of the sample holder (to about 0.3°). That is, the beam is perpendicular to the axis, about which the sample rotates for changing the angle of incidence (Figure 5).

E. Angle of Incidence Calibration

For the angle of incidence measurement to be accurate, not only must the beam be perpendicular to the sample axis of rotation, but it also must pass through that axis, and the zero rotation position must be

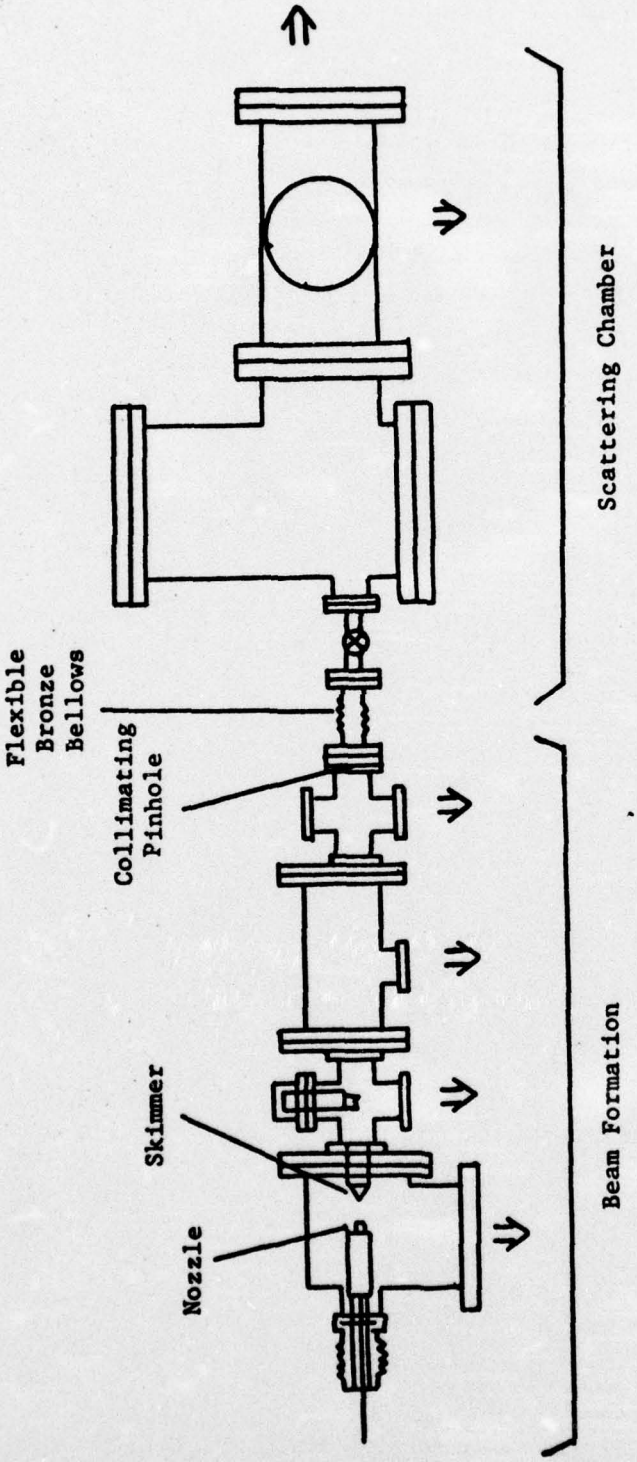

Figure 4. Diagram of the Apparatus.

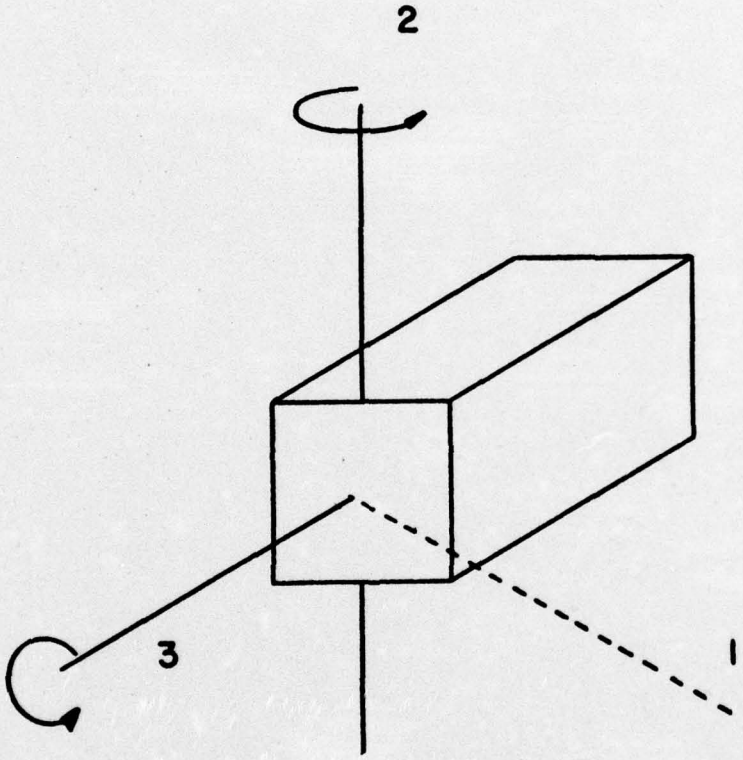

Figure 5. Diagram of Sample Movement.

1. Beam Direction.
2. Angle of Incidence Rotation Axis.
3. Azimuthal Angle Rotation Axis.

known. The beam formation end of the system can be moved via the fine adjustment screws, which are calibrated. The position can also be checked by an external micrometer which measures the relative horizontal position of the collimating pinhole with respect to the scattering chamber. With the sample pushed back into the holder, the sample holder is rotated so that its face is parallel to the beam. This is done by placing the beam in such a position that it is partially blocked by the sample holder and the detector is in the beam. The sample holder is rotated until maximum intensity results at the detector. At this point, the beam is parallel to the sample holder at an incident angle of 90°. The beam is then slowly moved perpendicular to the sample holder, with intensity measurements made at various positions, the detector being readjusted for maximum intensity at each point. The range covered is from full, unobstructed intensity to almost total blockage by the sample holder.

The sample holder is then rotated 180°, and the same procedure is followed, moving the beam in the other direction. Once this is done, the intensity as a function of position is plotted for both cases. Figure 6 is such a plot. From this, the midpoint between the two sample holder positions, which is the rotation axis, can be found and the beam can be placed there.

It should be noted that all of the calibration was done with the sample pushed back flush with the holder. This means that the angle of incidence has been calibrated with respect to the holder - not precisely the sample.

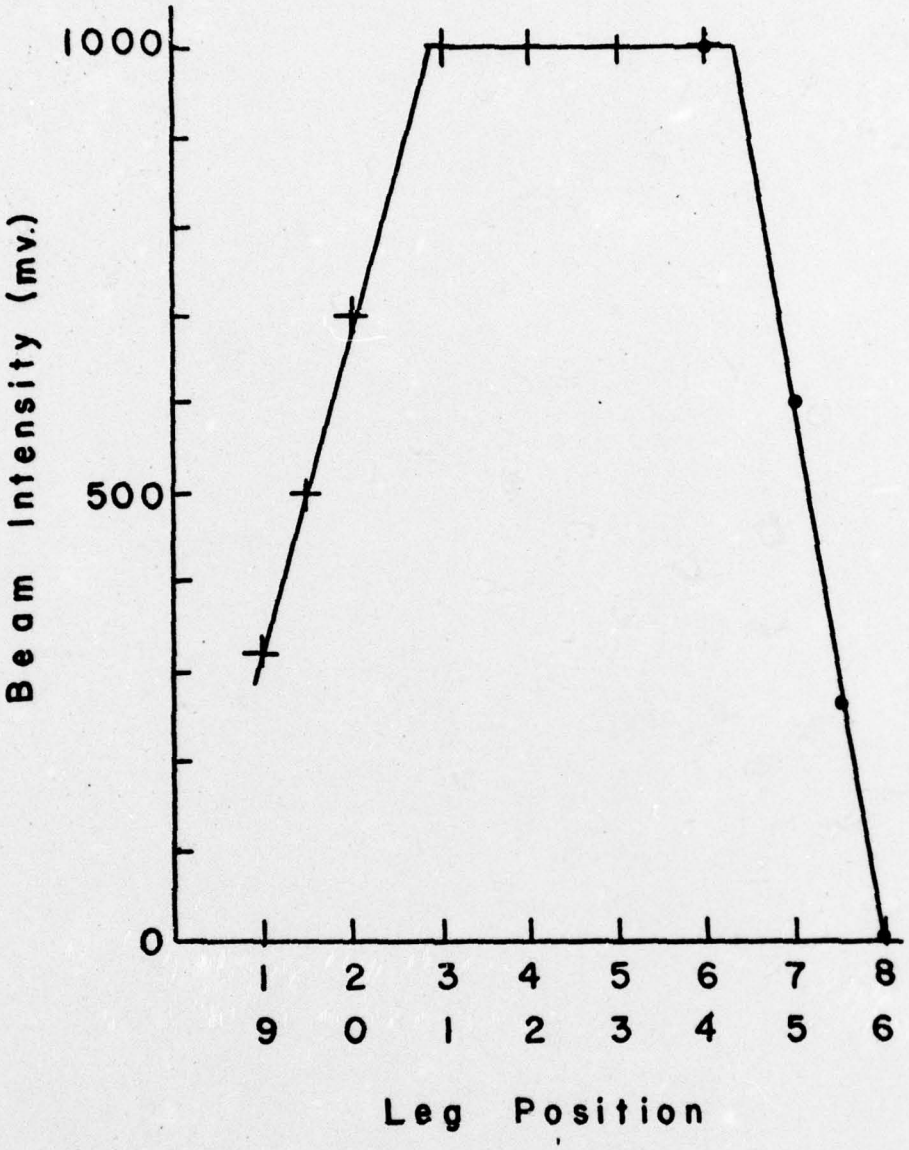

Figure 6. Incident Angle Calibration.

F. Azimuthal Angle Calibration

The calibration of the azimuthal angle can be accomplished using the crystallographic symmetry of the surface. Since it is known that about certain azimuthal positions the reflected features will be symmetrical, these positions can be used to accurately calibrate the azimuthal angle scale. All that is needed is to plot the reflected intensity vs. the azimuthal angle and then find the symmetry point from the shape of the graph (Figure 7).

G. Preliminary Adjustments

The procedure for taking data is as follows: the sample is cleaved in vacuum and then pushed back so that it is flush with the sample holder, then the sample holder is placed in the 90° incident angle position, and the detector placed in the direct beam. The sample is advanced a known amount by means of a spacer placed on the advancing mechanism. This is done to place the surface in the beam and close to the axis.

H. Beam Location

The desired beam is then located by the following calculation: First the beam must be inside the Ewald sphere for the experimental conditions. Once this is determined, the incident $\vec{K}_{\parallel}$ wavevector is drawn so that it terminates at the origin of a $\vec{K}_x\vec{K}_y$ diagram (Figure 8). Then $\vec{K}'_{\parallel}$, the parallel component of the diffracted beam, is drawn to the desired diffraction point. The angle between the plane of the surface and the diffracted beam can be calculated by knowing the length of $\vec{K}'_{\parallel}$, and that $|\vec{k}'| = |\vec{k}|$. The height from the plane of the

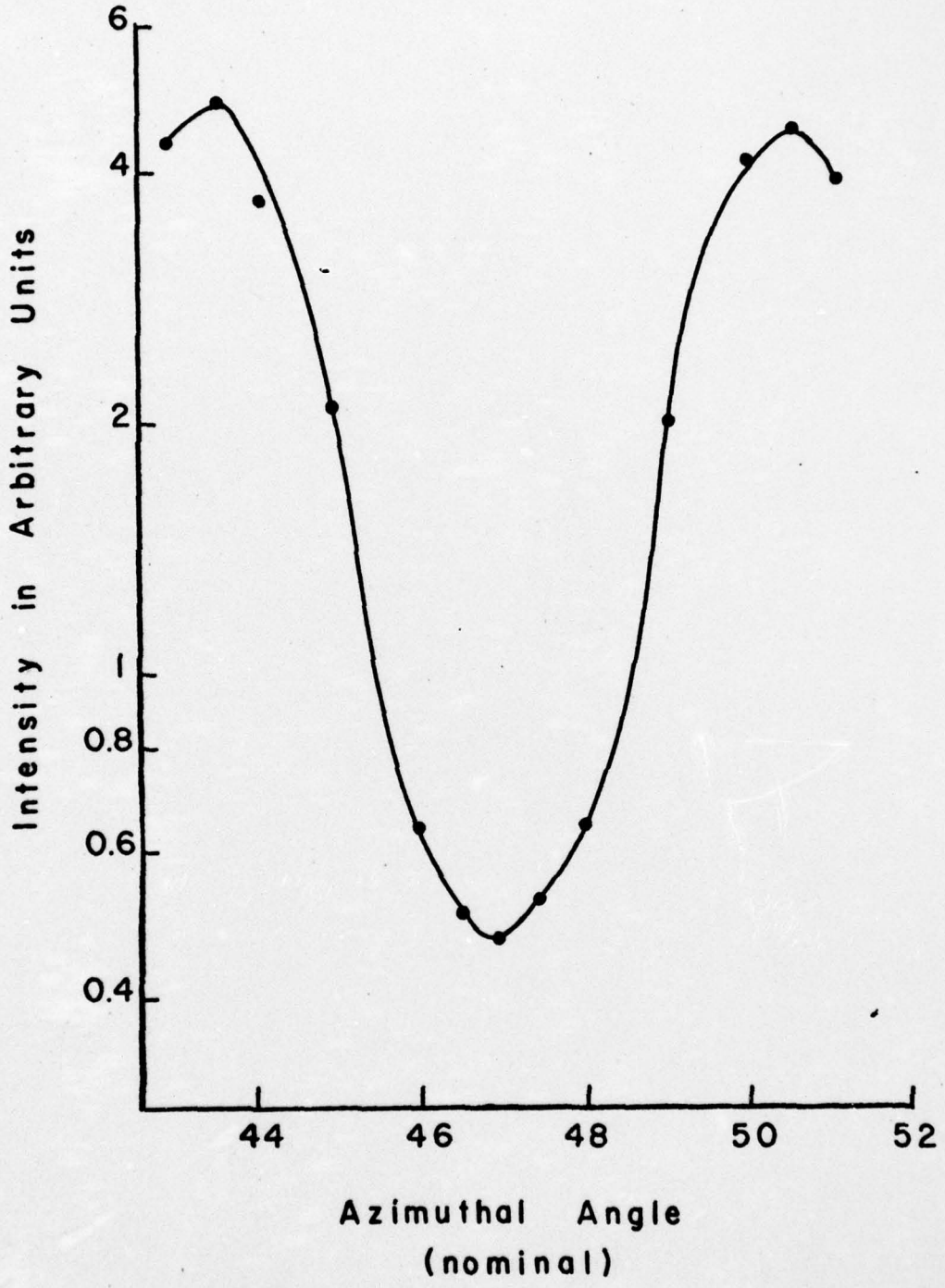

Figure 7. Azimuthal Angle Calibration Showing True $\phi = 45°$ at Nominal $\phi = 47°$.

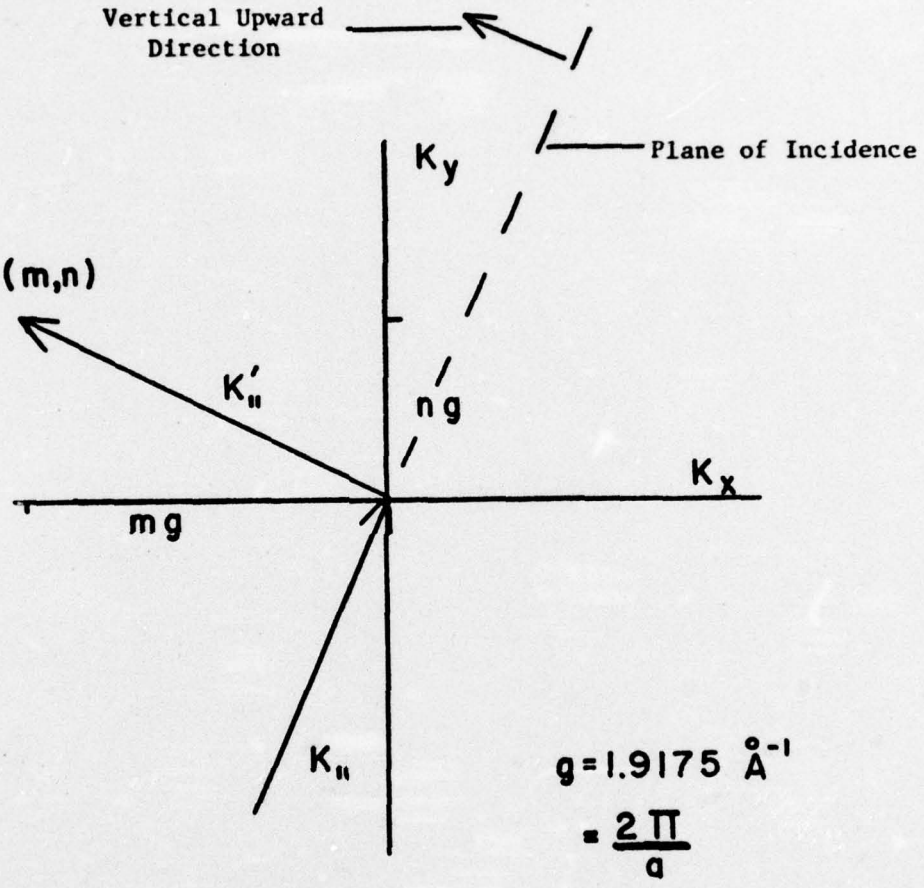

Figure 8. Location of the (m,n) Diffracted Beam Shown in a Projection onto a Plane Parallel to the Crystal Surface.

surface normal and the incident beam can be calculated by knowing the radius of the detector swing and the angle between $\vec{K}_{\parallel}$ and $\vec{K}'_{\parallel}$.

I. Measurement Procedure

Once the desired beam is located, it is followed, usually for different incident angles at fixed azimuth. As mentioned earlier, the incidence angle was calibrated with respect to the sample holder. However, if the cleave is imperfect or if the sample moves in the holder, then the incident angle with respect to the sample would be wrong. To find the true angle of incidence, the four-fold symmetry of the surface is used. Once a feature is located in one azimuth, it can then be located in three other crystallographically equivalent azimuths (Figure 9). The apparent incident angles will be different for the same feature in different azimuths if the surface is not parallel to the holder, but the average of these angles should be the correct angle of incidence. In practice, it was found that two equivalent azimuthal positions, 180° apart, were often sufficient to fix the incident angle.

This procedure assumes that the beam is hitting the same point on the sample. In order to insure this, the beam must be hitting the center of the sample. Since it is already on the rotation axis, to accomplish this, the sample is pushed out until it completely blocks the beam. The beam is then moved above and below the sample. These positions are noted, and the beam is placed midway between them.

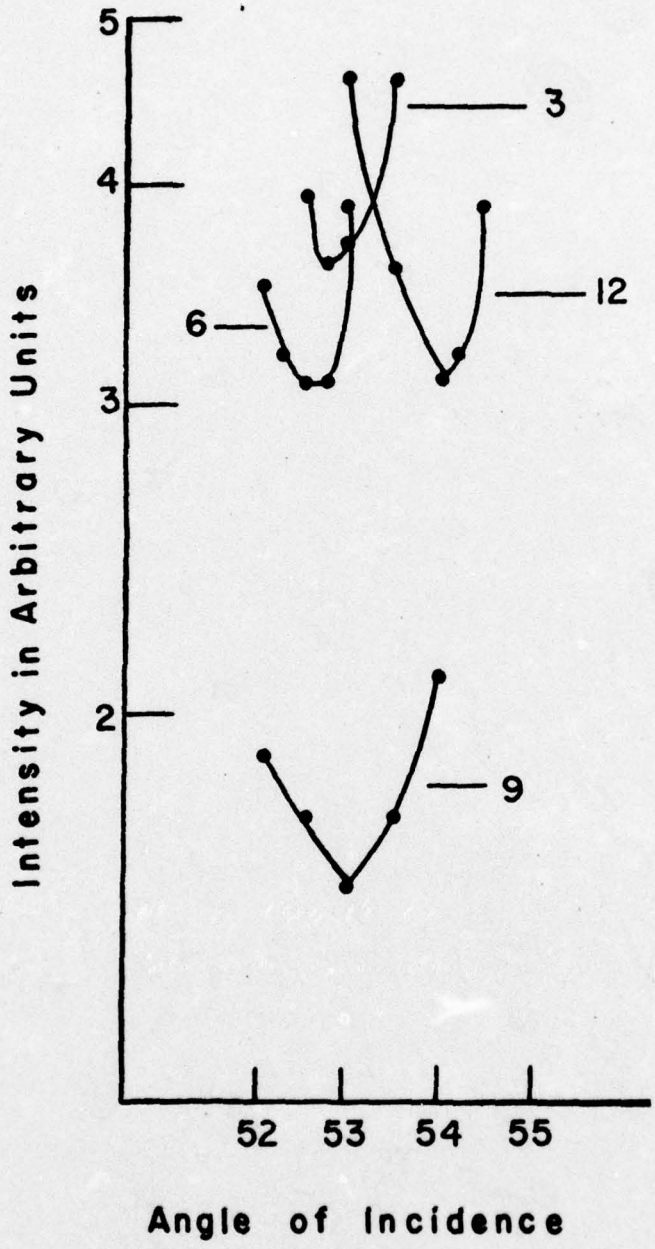

Figure 9. The Same Feature Shown in Four Equivalent Azimuthal Positions. The Numbers Represent "Clock Positions" of a Reference Mark on the Sample Holder.

III. EXPERIMENTAL RESULTS

A. Selective Adsorption

The early part of this study was devoted to finding the selective adsorption bound state energies. As mentioned earlier, data are taken by recording intensities vs. angle of incidence for the reflected intensity.

Table 2 contains the data obtained. These values are for the reflected intensity from a NaF (001) surface at room temperature. Table 3 is a summary of the data showing the incident wavevector magnitude, the incident and azimuthal angles, the position in the k_x, k_y plane, and the ϵ value for each minimum found.

If these points are plotted in k_x, k_y space, then, according to Equation (1), circles centered around $-\vec{G}_{mn}$ should result. *Figure 10* is such a plot for the values obtained. The $\vec{G}_{mn}$ vectors in this case are $\vec{G}_{10}$ and $\vec{G}_{01}$. The fourth energy level can only be resolved at azimuthal angles close to zero. That, combined with the fact that the fourth level is so close to the dissociation limit, is why so few points can be obtained for it.

From Equation (1), it can be seen that if the data are plotted in the $\vec{G}$ plane (reciprocal space) circles will again result, this time centered about $-\vec{K}_{11}$. This is just the two-dimensional representation of the Ewald sphere diagram. Figure 11 is an Ewald sphere representation for the deepest energy level.

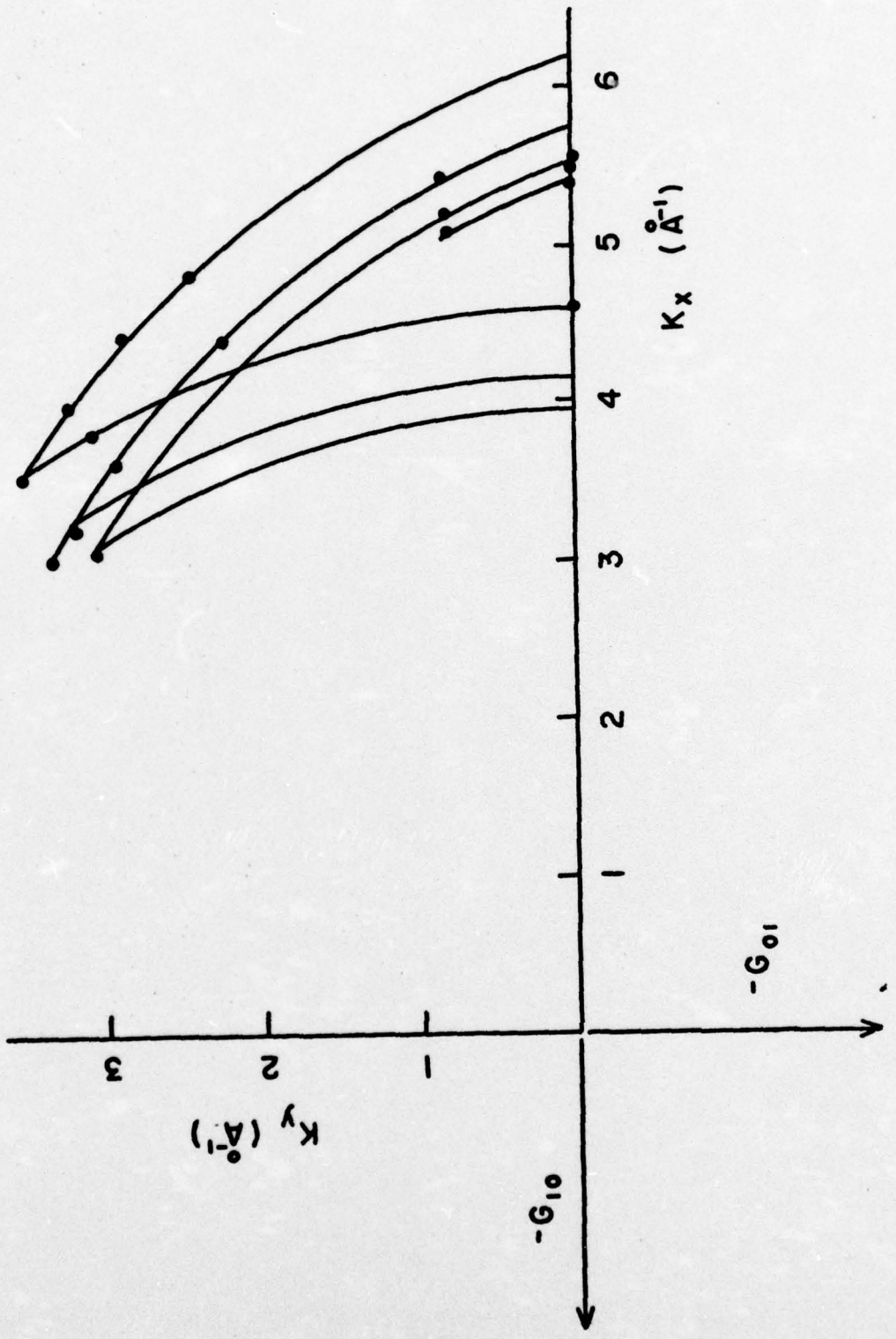

Figure 10. Selective Adsorption Minimum Points in the $K_x K_y$ Plane. The Lines are Circles Centered about the $-G_{10}$ and $-G_{01}$ Reciprocal Lattice Points.

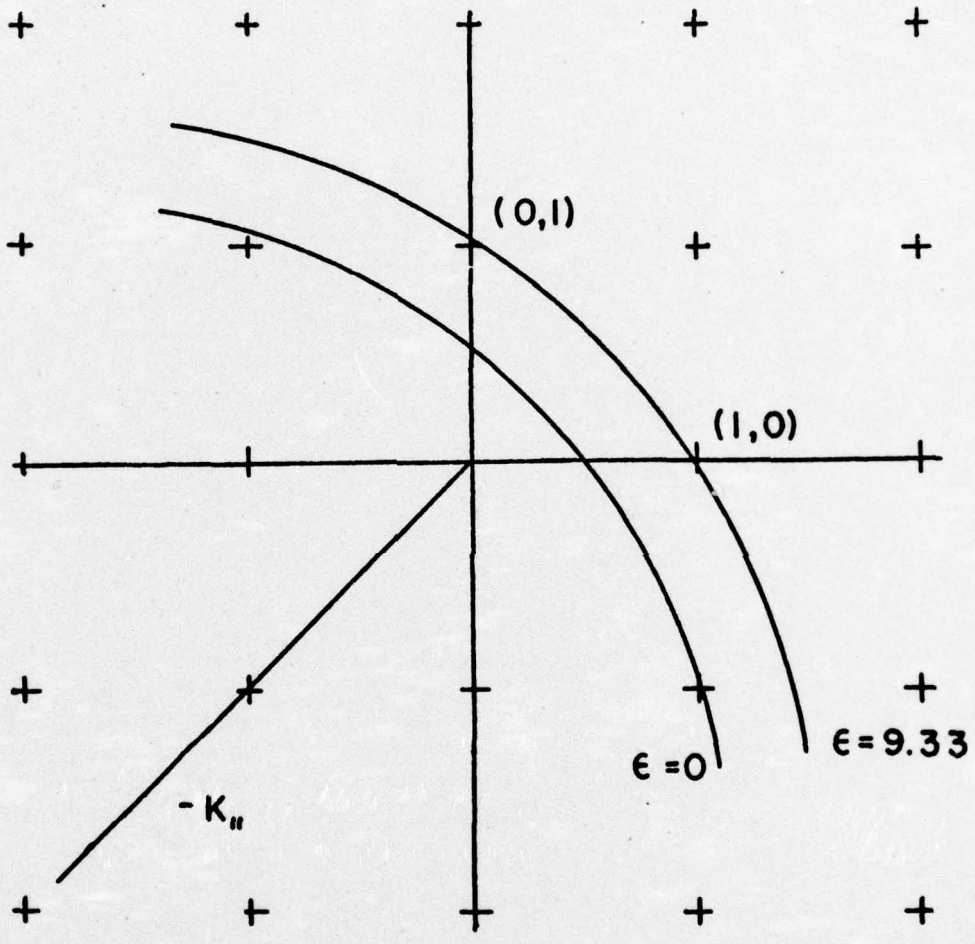

Figure 11. Ewald Sphere Diagram for Conditions Giving Selective Adsorption in the Deepest Energy Level at $\phi = 45°$.

This type of representation is quite useful since it displays several types of information. The points lying inside the Ewald sphere give the possible diffraction beams. The points lying on the energy-level circles give the bound-state transitions. (In the case of Figure 11 the (10) and (01) transitions are occurring simultaneously; i.e., they are degenerate.) Since the incident and azimuthal angles can be obtained quite easily from this type of diagram, conditions can readily be set up and tested experimentally. For this purpose, a transparency with the Ewald sphere and the energy level circles were made and fitted onto a stationary reciprocal lattice grid.

Table 1 shows the values of the four bound state energy levels found in this study compared to values others have obtained. If these values are interpreted according to LeRoy's method, that is, E 1/6 vs. η where η is proportional to the vibrational quantum number, a straight line should result. Figure 12 is such a plot, and indeed the points do fall on a straight line. The error bars are omitted on the fourth energy level because, due to its small value, they are off the graph. Further interpretation similar to LeRoy's gives a well depth of -7.49 mev, a value for c_3 (the coefficient of the z^{-3} term in the potential) of -140.43 mev $\mathring{A}^3$ and the total number of bound states as 7. Using this information, a 12-3 form of the potential was calculated Figure 13.

B. Diffraction

The second part of this study was devoted to the study of diffracted beams, specifically, the conditions at which the maxima predicted by Chow and Thompson occur.

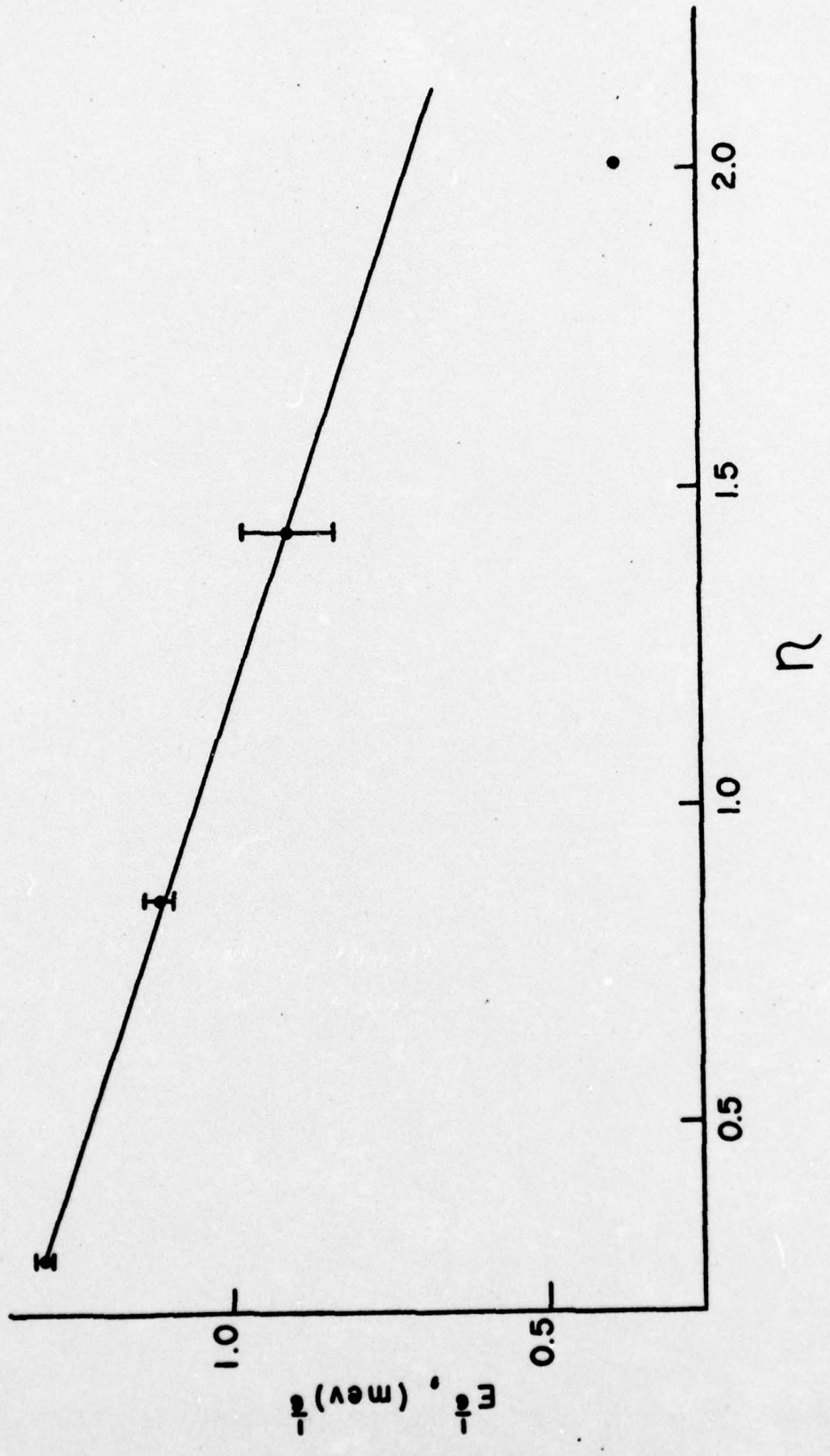

Figure 12. Energy Level Values Plotted According to the Method Described by LeRoy.(15)

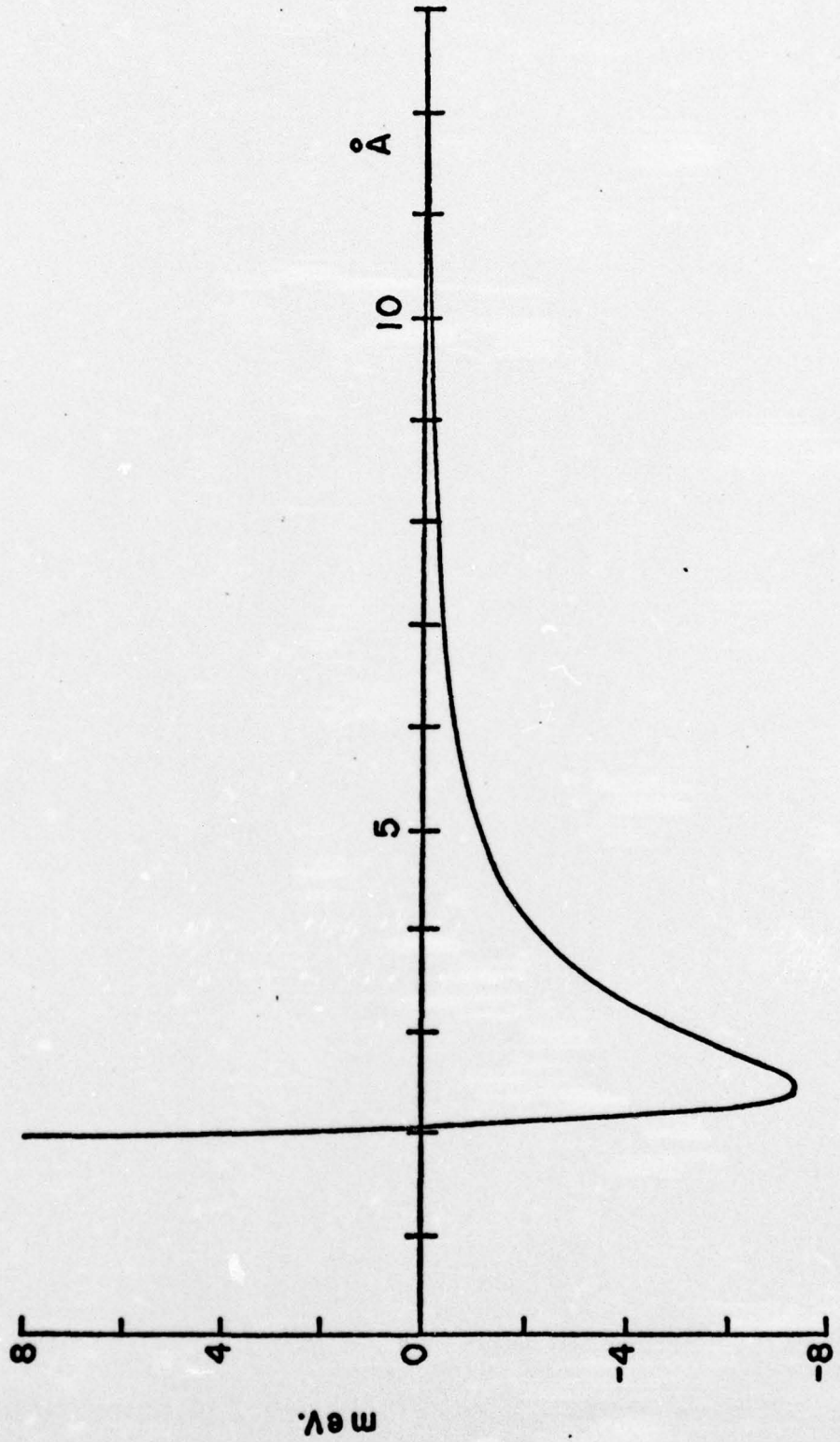

Figure 13. 12-3 Form of the Potential:

$$V = \frac{97264 \text{ mev } \mathring{A}^{12}}{Z^{12}} - \frac{140.43 \text{ mev } \mathring{A}^{3}}{Z^{3}}$$

Data for several diffracted and reflected intensities, as a function of the incident angle, for an azimuthal angle of 45°, is contained in Table 4. Figure 14 is a plot of the data. The reflected intensity shows the selective adsorption bound state minima, and most of the diffracted beams also show minima at the same incident conditions. The exception is the $(\bar{1}1)$ beam which shows distinct maxima.

The corresponding Ewald sphere diagram is shown in Figure 15, using the first energy level as an example. From this diagram, it can be seen that the bound state transitions to the (01) and (10) points are degenerate. Since the $(\bar{1}1)$ beam showed a maximum for these conditions, then, according to Chow and Thompson, there are possible transitions from the (01) and (10) bound states to the $(\bar{1}1)$ beam, shown as dotted vectors on Figure 15.

To determine which of these possible transitions is taking place, the (01) and (10) bound state transition degeneracy must be removed. To accomplish this, the azimuthal angle was moved off the symmetry direction to 48°, and the splitting of the two transitions for the second level was observed. Data for the intensity as a function of the incident angle for the reflected and the $(\bar{1}1)$ beams is contained in Table 5. Figure 16 is a plot of this data and clearly shows the splitting into two minima, the one at 53° corresponding to the (10) transition, and the one at 51° to the (01) transition. The $(\bar{1}1)$ beam shows a maximum for the (01) transition. Figure 17 is the Ewald sphere diagram for the (01) transition. This illustrates the transitions taking place, first to the (01) bound state, then another transition to the $(\bar{1}1)$ beam, since that beam shows a maximum at these conditions. It can also be concluded that

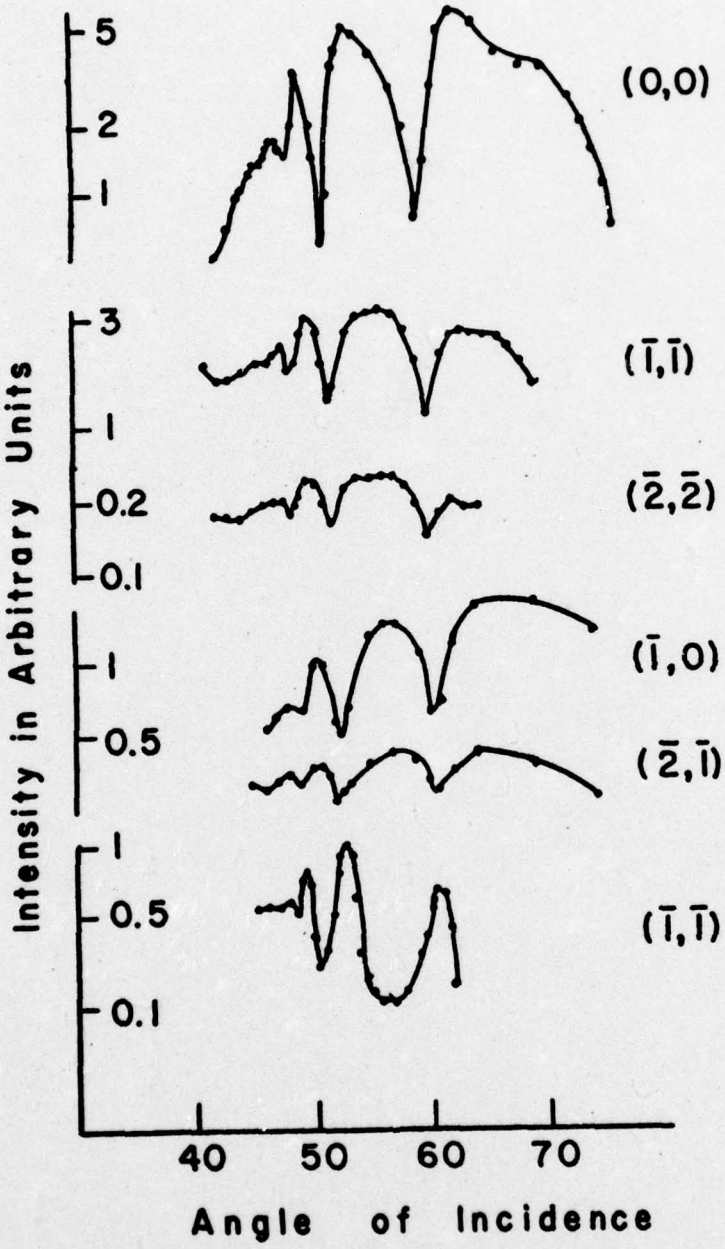

Figure 14. Intensities of Various Diffracted Beams at $\phi = 45°$.

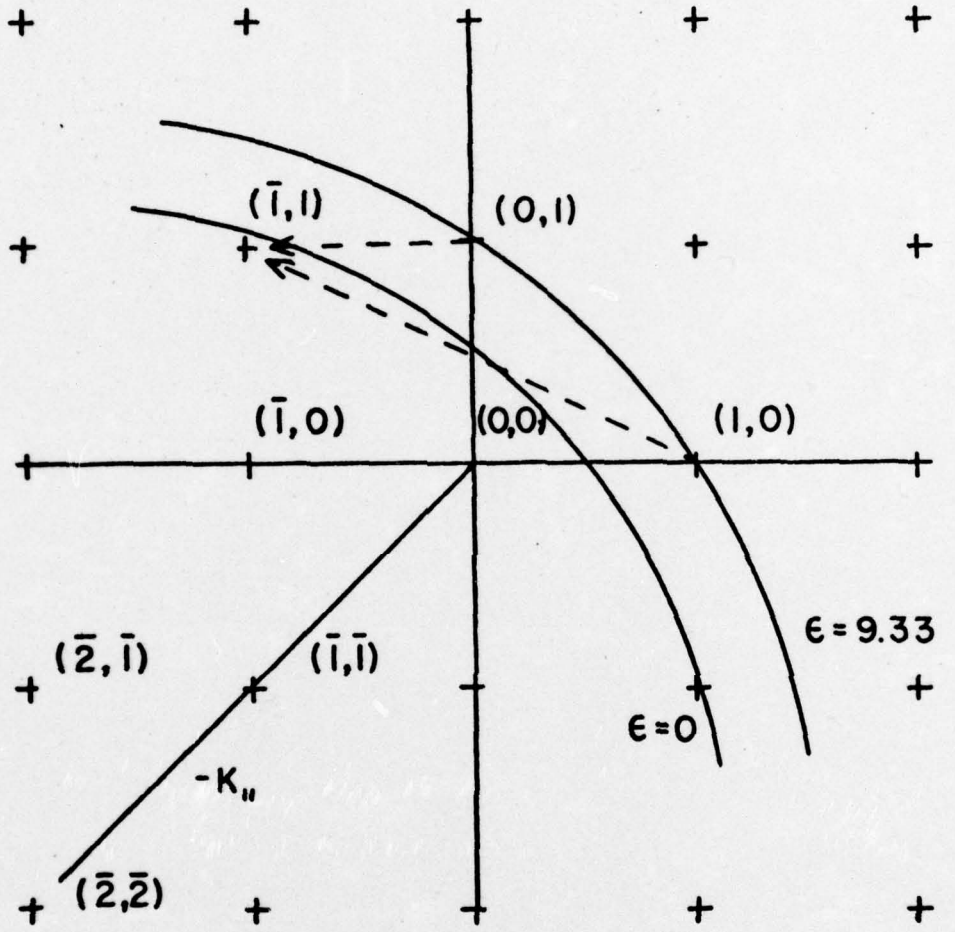

Figure 15. Ewald Sphere Diagram for the Deepest Level ($\varepsilon = 9.33$) at $\phi = 45°$ Including Possible Transitions from Bound States to the $(\bar{1}1)$ Diffracted Beam.

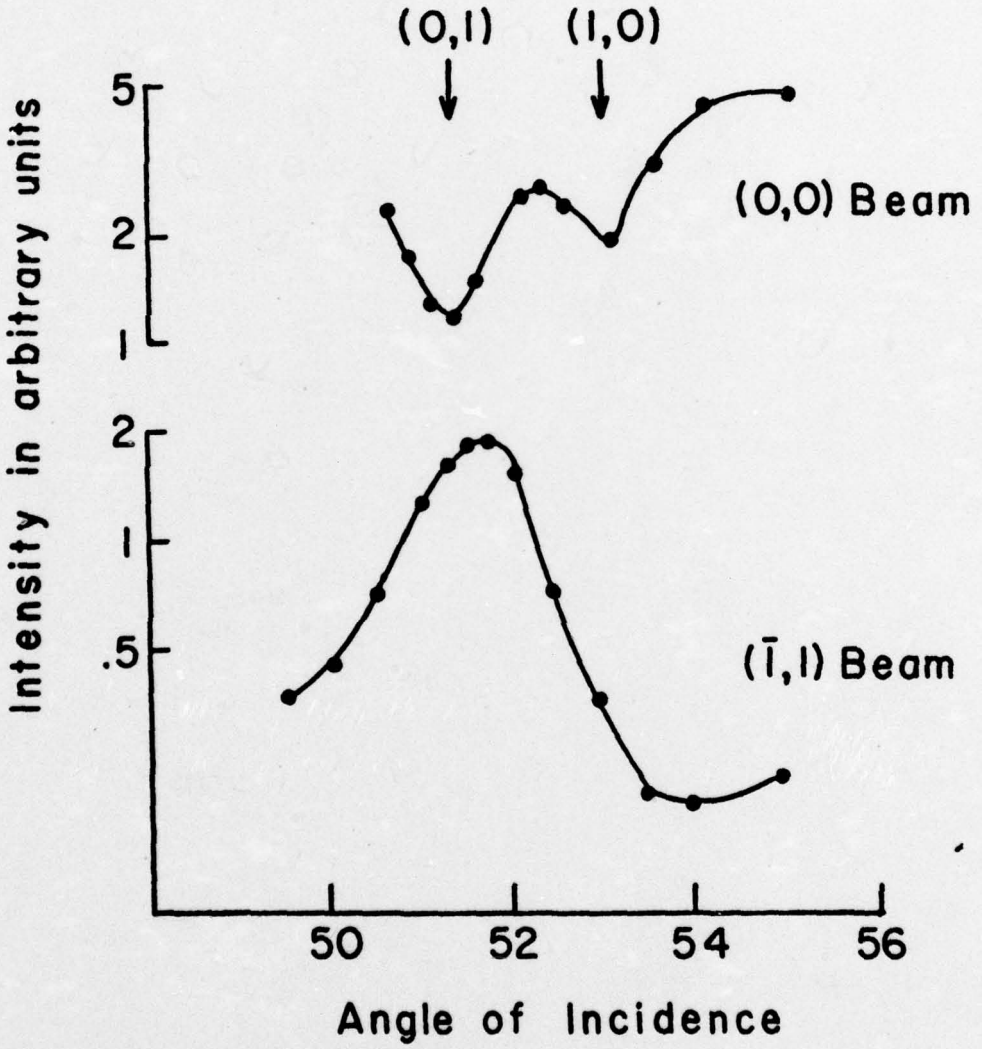

Figure 16. The Separation of the (01) and (10) Bound State Transitions for the (0.0) and ($\bar{1}$1) Beams at $\phi = 48°$.

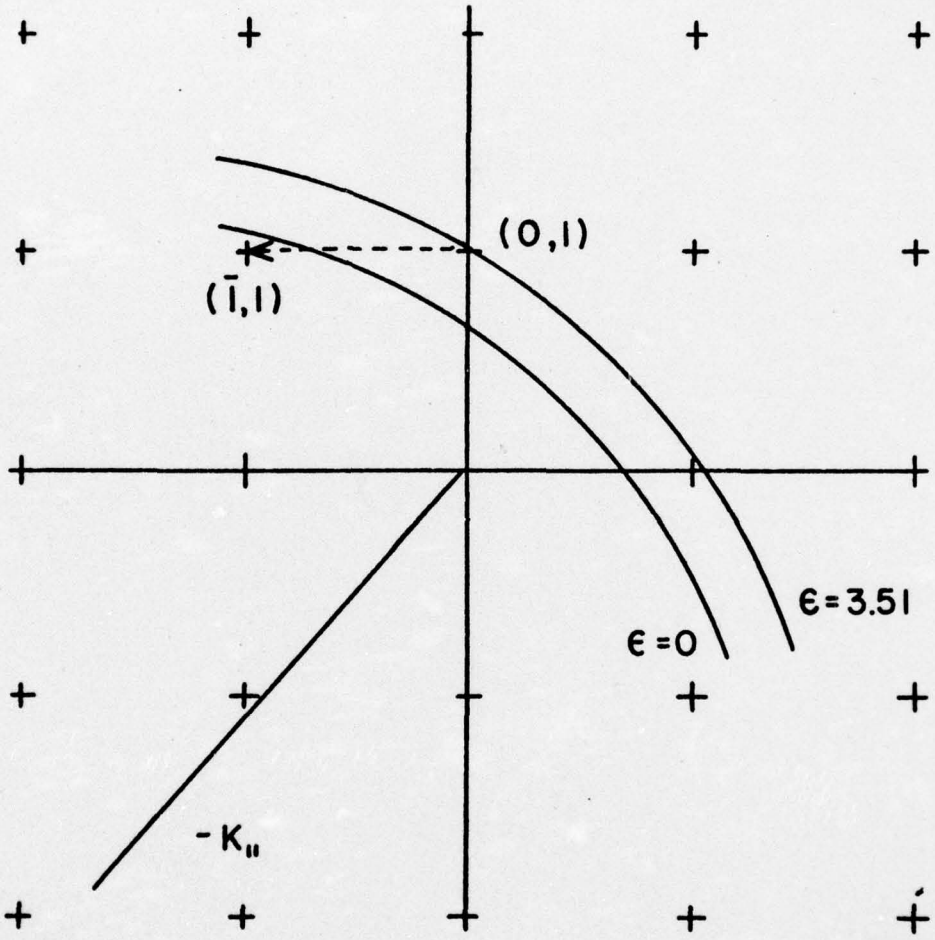

Figure 17. Ewald Sphere Diagram for the Second Level (ϵ = 3.51) at ϕ = 48° Including the Transition from the (01) Bound State to the ($\bar{1}1$) Diffracted Beam.

no transition is taking place from the (10) bound state to the $(\bar{1}1)$ beam since both the reflected and $(\bar{1}1)$ diffracted beams show minima for that transition.

If the azimuth is rotated to 0°, bound state transitions to the (01) and $(0\bar{1})$ states of the third and fourth levels will occur near glancing incidence. Again, to split the degeneracy, the azimuth was set at -1° and data taken for the (00), $(\bar{1}1)$ and $(\bar{2}1)$ beams (Table 6). This data is plotted in Figure 18, which shows the splitting of the (01) and $(0\bar{1})$ bound state transitions for the third level. The (01) transition, which occurs at an incident angle of 76°, produces maxima in the $(\bar{2}1)$ and $(\bar{1}1)$ beams, whereas the $(0\bar{1})$ transition, which occurs at 73.5°, produces minima. Figure 19 is the Ewald sphere diagram for the (01) transition showing the transitions from the (01) bound state to the $(\bar{1}1)$ and $(\bar{2}1)$ beams, both of which exhibit maxima at these conditions. Again, it can also be concluded that no transitions are taking place from the $(0\bar{1})$ bound state to the $(\bar{2}1)$ or $(\bar{1}1)$ beams.

Summing up, several maxima in diffracted beams have been seen. They have resulted from transitions of the following types: at $\phi = 48°$ from (01) to $(\bar{1}1)$ and at $\phi = -1°$ from (01) to $(\bar{2}1)$ and from (01) to $(\bar{1}1)$. No diagonal vectors in the second step have been observed.

C. Splitting of Degenerate Levels

The degeneracy of two bound state transitions is seen by the crossing of circles in the $k_x k_y$ plane as was discussed above. For example, Figure 10 shows degenerate (01), (10) transitions along the $\phi = 45°$ line.

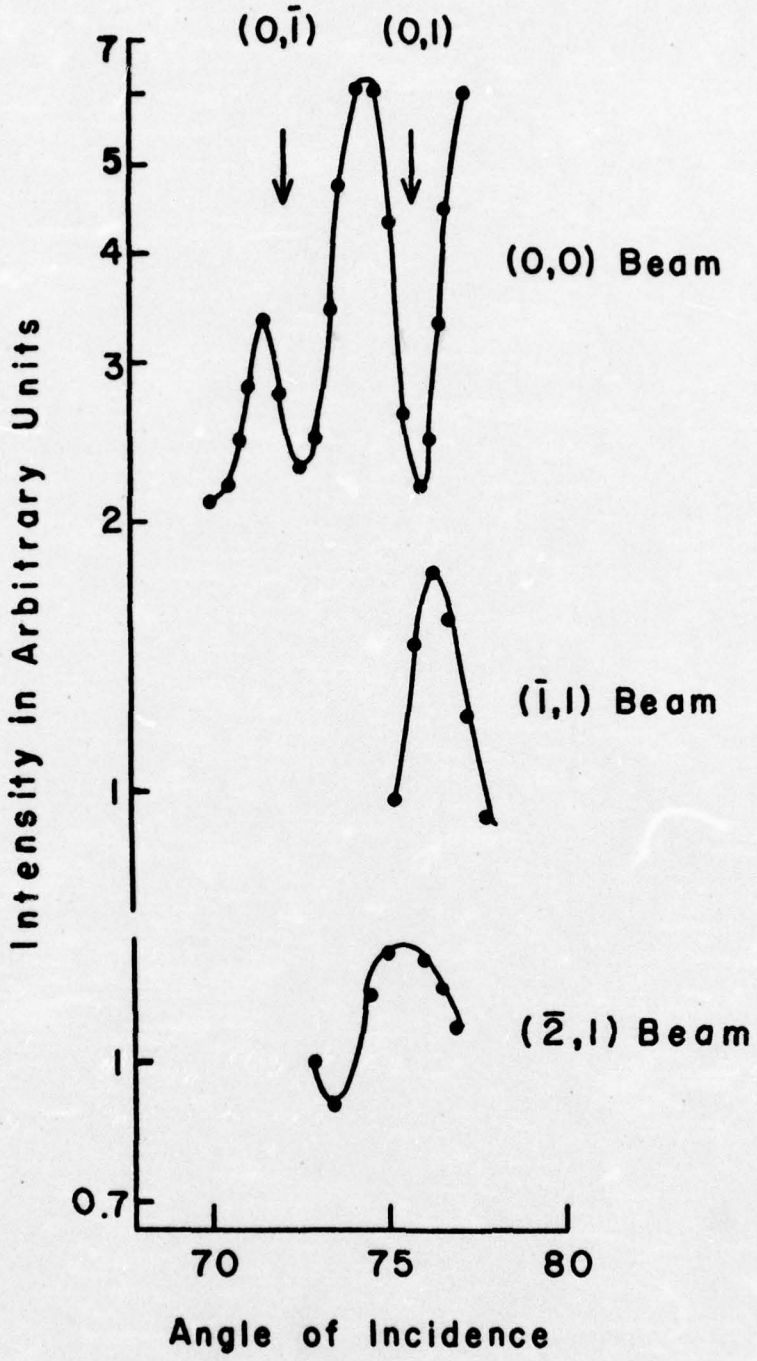

Figure 18. The Separation of the (0$\bar{1}$) and (01) Bound State Transitions for the (00), ($\bar{1}$1) and ($\bar{2}$1) Beams at $\phi = -1°$.

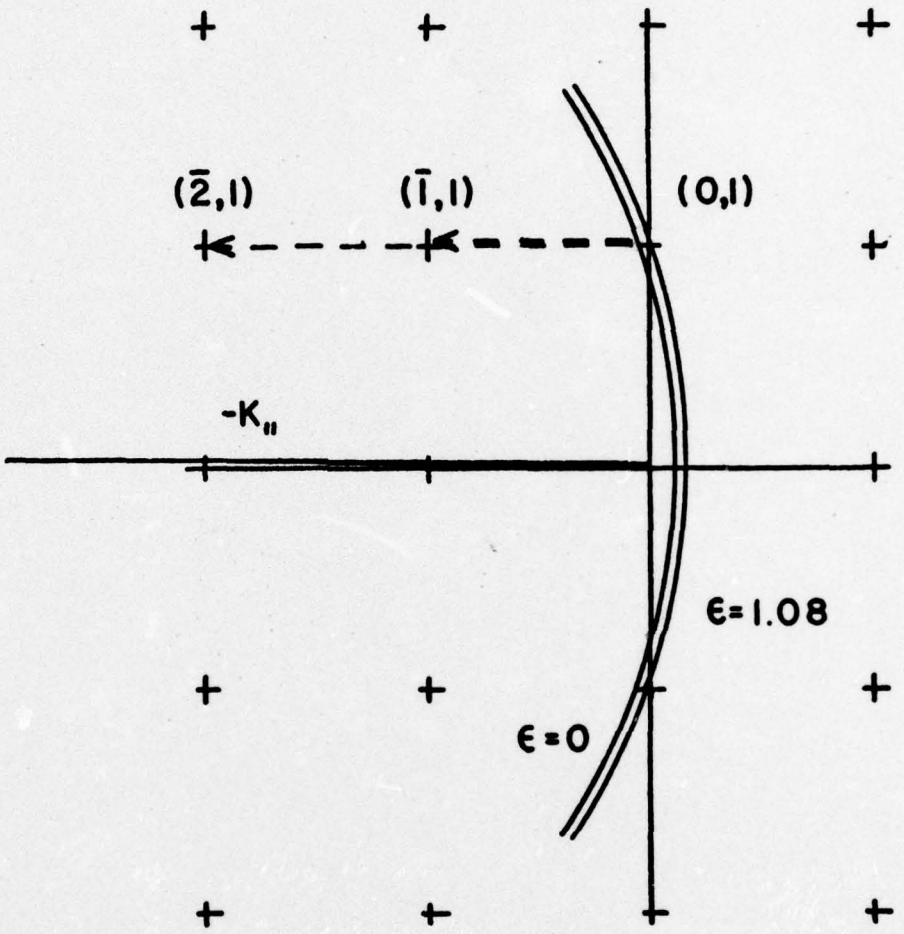

Figure 19. Ewald Sphere Diagram for the Third Level ($\varepsilon = 1.08$) at $\phi = -1°$ Including the Transitions from the (01) Bound State to the $(\bar{1}1)$ and $(\bar{2}1)$ Diffracted Beams.

Chow and Thompson[17] have predicted that, in certain cases, the levels will split and no longer be degenerate. That is, the curves will deviate from circles and will not cross. Specifically, they predicted that the (10) and $(1\bar{1})$ transitions to the deepest level around $\phi = 10°$ will show such splitting.

To find such behavior, the sample was cooled to approximately 80°K. The reflected intensity was scanned for various angles of incidence at several azimuthal angles. Table 7 contains the observed data and Figure 20 is a plot of that data showing the minima observed.

If the minima points are plotted in the k_x, k_y plane, a graph such as Figure 21 results. From Figure 21, it can be seen that the degeneracy indeed does not occur; that is, the curves do not cross but remain separate asymptomatically approaching the expected circles.

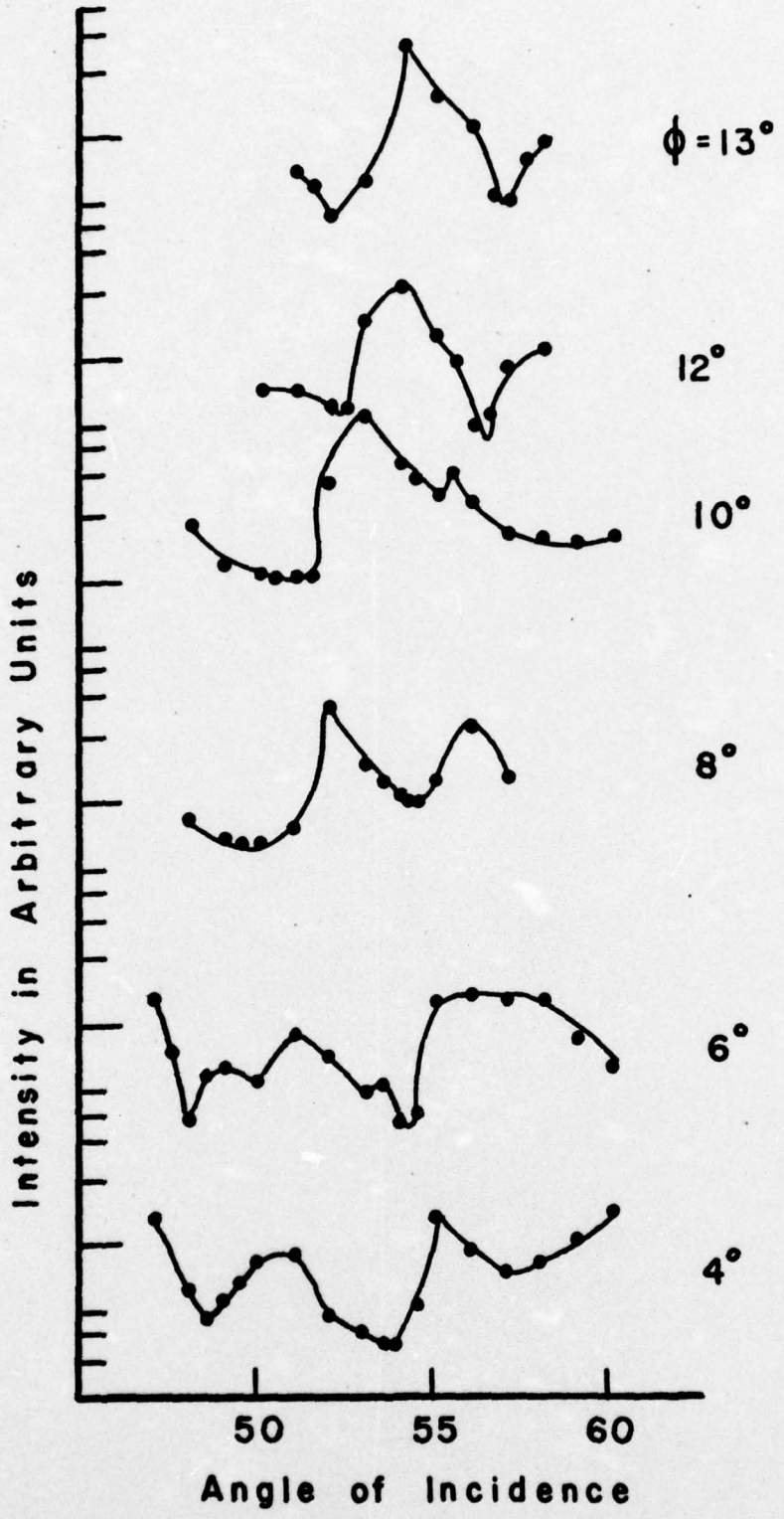

Figure 20. Reflected Intensity at Various Azimuthal Angles.

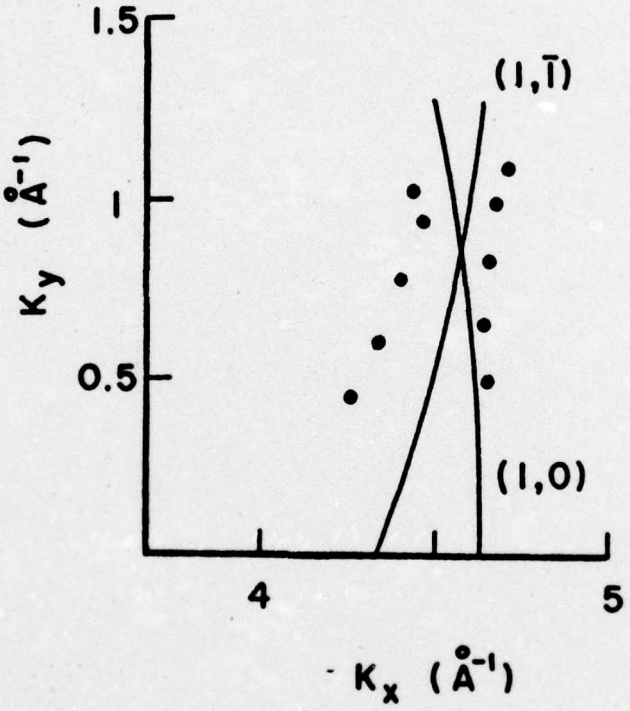

Figure 21. The $K_x K_y$ Plot Showing the Expected Paths of the $(1\bar{1})$ and (10) Bound State Transitions (Solid Lines) and the Actual Points.

IV. CONCLUSIONS

The main results of this study are as follows:

(1) Four bound state energy levels for He on the (001) surface of NaF have been found and values obtained. The first three levels which had been observed by others are in reasonable agreement with previously found values. The values fit well the prediction by LeRoy that the sixth root of the energy is linearly proportional to the vibrational quantum number.

(2) Several examples of maxima and minima in diffracted beams have been observed. These observations are consistent with predictions made by Chow and Thompson, thereby giving evidence that the multiple scattering effects do occur.

(3) At least one example of a degeneracy splitting has been observed, which again is consistent with predictions by Chow and Thompson.

TABLE 2

Reflected Intensity Data for Selective Adsorption Energy Levels

5/12	ϕ = 45°	1st Level	K = 5.820 $\AA^{-1}$
	Sample Angle (deg)	Intensity (mv)	
1200	110	13	
	110.5	11	
	111	9.1	
	111.5	6.1	
	112	3.0	
	12.5	4.1	
	112.25	2.8	
600	110	3.4	
	110.5	2.4	
	111	3.0	
	110.75	2.1	
900	110	1.7	
	110.5	1.5	
	111	2.2	
	110.25	1.4	
300	110	10	
	110.5	7.1	
	111	4.4	
	111.5	2.6	
	112	6.0	
	111.25	3.2	
	111.75	3.5	

TABLE 2 (Continued)

5/12	ϕ = 39°	1st Level	K = 5.820 $\AA^{-1}$
	Sample Angle (deg)	Intensity (mv)	
1200	116	18	
	115	12	
	114.5	17	
	115.5	11	
	115.25	11	
600	116	16	
	115.5	16	
	115	14	
	114.5	12	
	114	8.3	
	113.5	6.2	
	113	7.1	
	113.25	6.2	
900	115	6.8	
	114.5	5.8	
	114	4.5	
	113.5	3.5	
	113	3.6	
	113.25	3.3	
300	116	24	
	115.5	19	
	115	13	
	114.5	8.3	
	114	10	
	114.25	8.6	

TABLE 2 (Continued)

5/12	ϕ = 33°	1st Level	K = 5.820 $\mathring{A}^{-1}$
	Sample Angle (deg)	Intensity (mv)	
1200	119	9.1	
	118.5	4.4	
	118	7.2	
	118.25	5.4	
	118.75	5.0	
600	118	6.7	
	117.5	5.2	
	117	3.1	
	116.5	2.0	
	116	2.5	
	116.25	2.2	
	116.75	2.1	
900	118	2.1	
	117.5	1.5	
	117	1.7	
	117.25	1.5	
300	119	12	
	118.5	9.9	
	118	6.2	
	117.5	2.2	
	117	3.4	
	117.25	2.5	
	117.75	3.3	

TABLE 2 (Continued)

5/12	ϕ = 27°	1st Level	K = 5.820 $\mathring{A}^{-1}$
	Sample Angle (deg)	Intensity (mv)	
1200	122	4.2	
	121.5	10	
	122.5	2.2	
	123	8.1	
	122.25	2.3	
	122.75	3.5	
600	122	3.6	
	121.5	2.7	
	121	1.8	
	120.5	1.0	
	120	1.0	
	120.25	.89	
	119.5	1.8	
900	122	1.3	
	121.5	.85	
	121	.96	
	121.25	.84	
300	122	6.4	
	121.5	3.4	
	121	.76	
	120.5	1.6	
	120.75	1.1	
	121.25	2.4	
	121	.72	

TABLE 2 (Continued)

5/17	ϕ = 45°	1st Level	K = 5.823 $\mathring{A}^{-1}$
	Sample Angle (deg)	Intensity (mv)	
1200	112	1.6	
	111.5	2.6	
	112.5	1.5	
	113	3.2	
600	113	6.3	
	112.5	5.2	
	112	3.8	
	111.5	2.0	
	111	1.2	
	110.5	1.4	
	110	2.2	
300	110	3.7	
	110.5	2.8	
	111	2.2	
	111.5	1.6	
	112	1.9	
	112.5	3.2	
900	112.5	2.4	
	112	1.5	
	111.5	1.0	
	111	1.2	
	110.5	1.6	

TABLE 2 (Continued)

5/17	ϕ = 39°	1st Level	K = 5.823 $\mathring{A}^{-1}$
	Sample Angle (deg)	Intensity (mv)	
900	115.5	3.0	
	115	2.4	
	114.5	2.1	
	114	2.2	
	113.5	2.5	
300	113	4.6	
	113.5	4.8	
	114	4.0	
	114.5	3.6	
	115	4.1	
	115.5	5.6	

5/17	ϕ = 33°	1st Level	K = 5.823 $\mathring{A}^{-1}$
	Sample Angle (deg)	Intensity (mv)	
300	116	3.7	
	115.5	4.1	
	116.5	3.1	
	117	2.2	
	117.5	1.6	
	118	1.7	
	118.5	2.7	
900	118.5	1.7	
	118	1.1	
	117.5	1.3	
	117	1.6	

TABLE 2 (Continued)

5/12	ϕ = 39°	1st Level	K = 5.820 $\AA^{-1}$
	Sample Angle (deg)	Intensity (mv)	
1200	109	16	
	108.5	18	
	109.5	14	
	110	12	
	110.5	9.3	
	111	13	
	110.75	10	
	110.25	10	
600	110	7.2	
	109.5	7.3	
	109	5.2	
	108.5	5.4	
	108.75	5.0	
900	110	3.2	
	109.5	2.3	
	109	2.5	
	109.25	2.3	
300	111	11	
	110.5	12	
	110	10	
	109.5	8.4	
	109	10	
	109.25	8.9	
	109.75	8.7	

TABLE 2 (Continued)

3/30	$\phi = 0$	1st Level	$K = 5.794\ \mathring{A}^{-1}$
	Sample Angle (deg)	Intensity (mv)	
130	107	8.5	
	106.5	11	
	106	15	
	105.5	11	
	105	2.5	
	104.5	1.6	
	104	1.8	
	104.25	1.7	
	103.5	2	
	104.75	1.4	
730	106	3.7	
	105.5	4.4	
	105	5.2	
	104.5	3.7	
	104	1.2	
	103.5	1	
	103	1.1	
	103.75	.98	

4/30	$\phi = 45°$	2nd Level	$K = 5.818\ \mathring{A}^{-1}$
	Sample Angle (deg)	Intensity (mv)	
1200	105	40	
	104.5	30	
	104	11	
	103.5	6	
	103	10	
	103.25	7.3	
	103.75	6.4	
	102.5	18	
600	101	23	
	101.5	16	
	102	9	
	102.5	6.2	
	103	18	
	102.75	10	
	102.25	5.8	

TABLE 2 (Continued)

4/17	ϕ = 9°	2nd Level	K = 5.818 $\AA^{-1}$
	Sample Angle (deg)	Intensity (mv)	
130	125	5.3	
	124	1.4	
	123.5	1.2	
	123	2.4	
	123.75	1.2	
	122.5	4.0	
	121.5	8.0	
	122	6.4	
730	125	10	
	124.5	8.7	
	124	6.4	
	123.5	3.7	
	123	2	
	122.5	1.3	
	122	2.2	
	121.5	4.4	

TABLE 2 (Continued)

5/13	ϕ = 45°	2nd Level	K = 5.821 $\mathring{A}^{-1}$
	Sample Angle (deg)	Intensity (mv)	
1200	104	3.1	
	103.5	3.6	
	103	4.6	
	104.5	3.9	
	104.25	3.2	
600	103	3.8	
	102.5	3.1	
	102	3.5	
	102.25	3.3	
	102.75	3.2	
900	103	1.6	
	102.5	1.7	
	102	1.9	
	103.5	1.7	
	104	2.1	
300	104	6.7	
	103.5	4.6	
	103	3.7	
	102.5	3.9	
	102.75	3.6	

TABLE 2 (Continued)

5/13	ϕ = 39°	2nd Level	K = 5.821 $\AA^{-1}$
	Sample Angle (deg)	Intensity (mv)	
1200	106	3.7	
	105.5	4.5	
	106.5	3.8	
	106.25	3.6	
	107	4.7	
600	106	5.6	
	105.5	4.5	
	105	3.7	
	104.5	3.4	
	104	3.8	
	104.75	3.4	
900	106	2.6	
	105.5	1.9	
	105	1.8	
	104.5	1.7	
	104	1.7	
300	106	4.7	
	105.5	3.7	
	105	4.0	
	105.25	3.6	

TABLE 2 (Continued)

5/13	$\phi = 27°$	2^{nd} Level	$K = 5.821\ \mathring{A}^{-1}$
	Sample Angle (deg)	Intensity (mv)	
1200	111	3.8	
	110.5	4.8	
	111.5	3.2	
	112	4	
	111.75	3.3	
600	111	3.8	
	110.5	3.1	
	110	2.3	
	109.5	2.1	
	109	2.3	
	109.75	2	
300	111	3.5	
	110.5	2.7	
	110	3.2	
	110.75	2.7	

TABLE 2 (Continued)

4/17	ϕ = 48°	2nd Level	K = 5.818 $\mathring{A}^{-1}$
	Sample Angle (deg)	Intensity (mv)	
600	101	26	
	101.5	22	
	102	13	
	102.5	16	
	103	28	
	103.5	25	
	104	19	
	104.5	33	
1200	104.5	6.1	
	104	6.4	
	103.5	5.6	
	103	4.7	
	102.5	5.2	
	102	6.2	
	102.75	4.8	
	103.25	5.1	
	105	6.5	
	105.5	9.2	
	104.75	6.0	
	104.25	6.3	

4/30	ϕ = 45°	3rd Level	K = 5.818
	Sample Angle (deg)	Intensity (mv)	
1200	102	25	
	101.5	30	
	101	24	
	100.5	13	
	100	17	
	100.25	14	
	100.75	17	
	99.5	16	
	99	14	
600	99	15	
	99.5	14	
	100	29	
	99.75	23	
	99.25	13	
	98.5	18	

TABLE 2 (Continued)

4/17	ϕ = 9°	3rd Level	K = 5.818
	Sample Angle (deg)	Intensity (mv)	
130	118	7.8	
	117.5	3.5	
	117	4.1	
	117.25	3.6	
	116.5	5.7	
	116	5.4	
730	117.5	10	
	117	8.4	
	116.5	4.7	
	116.25	3.9	
	116	4.1	
	115.5	6.1	

4/30	ϕ = 0°	3rd Level	K = 5.818 $\AA^{-1}$
	Sample Angle (deg)	Intensity (mv)	
130	126	4.2	
	125.5	2.9	
	125	5.2	
	124.5	11	
	125.25	3.6	
	125.75	2.5	
	126.5	7.3	
	127	12	
730	126	14	
	125.5	7.4	
	125	4.3	
	124.5	5.4	
	124.75	4.5	
	125.25	5.7	
	124	8.6	

TABLE 2 (Continued)

3/20	$\phi = 0°$	3rd Level	$K = 5.794\ \mathring{A}^{-1}$
	Sample Angle (deg)	Intensity (mv)	
730	125.5	9.2	
	125	6.1	
	124.5	3.1	
	124	2.1	
	123.5	3.1	
	123	5.1	
	122.5	5.5	
130	126	17	
	125	9.4	
	124.5	15	
	124.75	11	
	125.25	8	
	125.5	9.1	
	124	22	

4/17	$\phi = 9°$	4th Level	$K = 5.818\ \mathring{A}^{-1}$
	Sample Angle (deg)	Intensity (mv)	
130	115.5	4.7	
	115	4.6	
	114.5	4.4	
	114	4.6	
	114.25	4.5	
	114.75	4.4	
730	115	6.2	
	114.75	5.7	
	114.5	5.6	
	114.25	5.4	
	114	5.4	
	113.75	5.6	
	113.5	5.8	
	113.25	6.0	

TABLE 2 (Continued)

4/30	$\phi = 0°$	4^{th} Level	$K = 5.818\ \mathring{A}^{-1}$
	Sample Angle (deg)	Intensity (mv)	
130	122	7.2	
	121.5	7.4	
	121	8	
	120.5	9.4	
	120	11	
	122.5	7	
	123	9.3	
	123.5	9	
	122.25	7.1	
	122.75	7.6	
730	122	4.6	
	121.5	4.4	
	121.75	4.4	
	121	4.2	
	120.5	4.6	
	120.75	4.4	
	121.25	4.3	
	120	5.0	

3/30	$\phi = 0°$	4^{th} Level	$K = 5.794\ \mathring{A}^{-1}$
	Sample Angle (deg)	Intensity (mv)	
730	122	4.3	
	121.5	2.8	
	121	2.5	
	120.5	2.6	
	120.75	2.5	
	120	2.8	
130	124	3.3	
	123.5	2.9	
	123	2.3	
	122.5	1.7	
	122	2.2	
	121.5	2.2	

TABLE 3

Summary of Selective Adsorption Data

Level	Date	$k(\mathring{A}^{-1})$	ϕ	Sample Angle	K_x, K_y	$\epsilon(\mathring{A}^{-2})$
1st	3/30	5.794	0	104.25	4.643, 0	9.463
	5/12	5.820	45	111.2	3.571, 3.571	9.006
			39	114.0	4.031, 3.265	9.230
			33	117.5	4.476, 2.907	9.437
			27	121.2	4.880, 2.487	9.338
			39	109.5	3.859, 3.174	9.218
	5/17	5.823	45	111.6	3.587, 3.587	9.263
			39	114.4	4.046, 3.277	9.442
			33	117.8	4.489, 2.915	9.597
					1st level avg	9.33 ± 0.17
2nd	4/30	5.818	45	102.88	3.236, 3.236	3.19
	4/17	5.818	48	104.25	3.119, 3.464	3.51
			48	102.63	3.052, 3.390	3.63
			9	123.05	5.454, 0.864	3.79
	5/13	5.821	45	103.13	3.249, 3.249	3.37
			39	105.08	3.664, 2.967	3.40
			27	110.5	4.470, 2.277	3.69
					2nd level avg	3.5 ± 0.21
3rd	4/17	5.818	9	116.83	5.242, 0.830	1.18
	4/30	5.818	0	125.38	5.603, 0	1.22
			45	99.8	3.099, 3.099	0.92
	3/30	5.794	0	124.63	5.559, 0	1.01
					3rd level avg	1.08 ± 0.14
4th	4/17	5.818	9	114.35	5.163, 0.813	0.013
	4/30	5.818	0	121.75	5.493, 0	0.002
	4/30	5.794	0	121.78	5.471, 0	0.004
					4th level avg	0.006 ± 0.005

TABLE 4

Intensity Data for Various Diffracted Beams

4/27	$(\bar{1}1)$ Beam	$\phi = 45°$	$k = 5.8\ \mathring{A}^{-1}$
Sample Angle (deg)		Intensity (mv)	
112		6.3	
111.5		6.7	
111		5.5	
110.5		4.3	
110		3.7	
109.5		3.0	
109		2.7	
112.5		4.4	
113		2.6	
111.75		6.4	
111.25		6.1	
108.5		2.5	
108		2.2	
107.5		2.2	
107		2.2	
106.5		2.2	
106		2.4	
105.5		2.8	
105		3.6	
104.5		6.1	
104		9.7	
103.5		10.0	
103		8.1	
103.25		9.5	
103.75		10.0	
102.5		5.1	
102		3.6	
101.5		3.1	
101		4.1	
100.5		7.3	
100		7.2	
100.25		8.0	
99.5		4.9	
99		5.9	
98.5		5.7	
98		5.6	
98.75		5.8	
99.25		5.6	
97.5		5.6	
97		5.6	
96.5		5.6	
96		5.6	

TABLE 4 (Continued)

12/29/75	(00) Beam	ϕ = 45°	k = 5.775 $\mathring{A}^{-1}$
Sample	Angle (deg)	Intensity (mv)	
	125	0.36	
	123	0.60	
	124	0.47	
	126	0.26	
	127	0.17	
	128	0.11	
	129	0.08	
	121	0.80	
	119	0.84	
	117	0.95	
	115	1.27	
	113	1.39	
	111	0.34	
	112	1.15	
	110	0.18	
	109	0.46	
	108	0.66	
	107	0.82	
	106	0.95	
	105	1.10	
	104	1.2	
	103	0.79	
	102	0.15	
	101	0.47	
	100	0.78	
	99	0.34	
	98	0.41	
	97	0.32	
	96.5	0.31	
	96	0.29	
	95.5	0.25	
	95	0.24	
	94	0.17	
	93	0.13	
	97.5	0.34	
	98.5	0.38	
	99.5	0.46	
	100.5	0.65	
	101.5	0.34	
	102.5	0.24	
	103.5	0.97	

TABLE 4 (Continued)

12/29/75	$(\overline{11})$ Beam	$\phi = 45°$	$k = 5.775\ \mathring{A}^{-1}$
Sample Angle (deg)		Intensity (mv)	
118		0.35	
117		0.38	
116		0.40	
115		0.39	
114		0.41	
113		0.40	
112		0.33	
111		0.18	
110		0.31	
109		0.42	
108		0.48	
107		0.51	
106		0.50	
105		0.49	
104		0.42	
103		0.24	
102.5		0.21	
102		0.28	
101.5		0.40	
101		0.46	
100.5		0.46	
100		0.40	
99.5		0.29	
99		0.28	
98.5		0.35	
98		0.33	
97.5		0.31	
97		0.30	
96.5		0.30	
96		0.29	
95		0.28	
94		0.26	
92		0.30	
93		0.25	

TABLE 4 (Continued)

12/29/75	$(\overline{22})$ Beam	$\phi = 45°$	$k = 5.775\ \mathring{A}^{-1}$
Sample Angle (deg)		Intensity (mv)	
115		0.038	
114		0.038	
113		0.040	
112		0.036	
111		0.028	
110		0.039	
109		0.046	
108		0.052	
107		0.053	
106		0.051	
105		0.052	
104		0.045	
103		0.032	
102		0.039	
101.5		0.048	
101		0.048	
100.5		0.049	
100		0.042	
99.5		0.036	
99		0.039	
98.5		0.040	
98		0.039	
97.5		0.038	
97		0.038	
96		0.037	
95		0.034	
94		0.034	
93		0.034	

TABLE 4 (Continued)

1/27/76	$(\bar{1}0)$ Beam	$\phi = 45°$	$k = 5.787\ \mathring{A}^{-1}$
Sample Angle (deg)		Intensity (mv)	
125		13.2	
120		18.2	
115		18	
113		12	
112		6.8	
111		6.2	
110		10.5	
108		14.7	
106		13	
104		6.4	
103.5		4.7	
103		5.6	
102		9.4	
101		9.3	
100		6.2	
99.5		6.3	
99		6.3	
98		5.9	
97		5.2	

1/27/76	$(\bar{2}\bar{1})$ Beam	$\phi = 45°$	$k = 5.787\ \mathring{A}^{-1}$
Sample Angle (deg)		Intensity (mv)	
108		4.7	
110		3.8	
111		3.1	
112		2.9	
113		3.4	
115		4.2	
120		3.7	
125		2.7	
106		3.8	
104		3.0	
103.5		2.8	
103		2.6	
102.5		3.3	
102		3.6	
101		3.5	
100		3.1	

TABLE 4 (Continued)

1/27/76	$(\overline{21})$ Beam	$\phi = 45°$	$k = 5.787\ \mathring{A}^{-1}$
Sample Angle (deg)		Intensity (mv)	
99		3.3	
98		3.2	
97		3.0	
96		3.0	

TABLE 5

Intensity Data for the Reflected and $(\bar{1}1)$ Diffracted Beams at $\phi = 48°$

$k = 5.818\ \mathring{A}^{-1}$

April 17		$(\bar{1}1)$ Beam $\phi = 48°$
	100.5	3.9
	101	4.6
	101.5	7.6
	102	13
	102.5	19
	102.75	19
	103	15
	103.5	7.3
	104	3.8
	104.5	2.1
	105	2.0
	106	2.3
		(00) Beam $\phi = 48°$
	106	53
	105	49
	104.5	35
	104	22
	103.5	26
	103.75	23
	103	28
	102.5	17
	102	14
	101.5	25
	101.75	19
	102.25	13

TABLE 6

Intensity Data for the Reflected $(\bar{1}1)$ and $(\bar{2}1)$ Beams at $\phi = -1°$

3/18	$(\bar{1}1)$ Beam	$\phi = -1°$	3rd Level
	Sample Angle (deg)	Intensity (mv)	
	126	14.5	
	126.5	17.5	
	127	15.5	
	127.5	12	
	128	9.3	
	125.5	9.7	

3/18	$(\bar{2}1)$ Beam	$\phi = -1°$	3rd Level
	Sample Angle (deg)	Intensity (mv)	
	128	1.1	
	127	1.3	
	126	1.35	
	125	0.95	
	124	1.0	
	124.5	0.9	
	125	1.0	
	125.5	1.2	

TABLE 6 (Continued)

3/18	(00) Beam	$\phi = -1°$	3^{rd} Level
	Sample Angle (deg)	Intensity (mv)	
	127	22	
	128	62	
	127.5	45	
	126.5	26.5	
	126	44	
	125.5	62	
	125	62	
	124.5	48	
	124	25	
	123.5	23.5	
	123	28	
	122.5	34	
	122	28.5	
	121.5	22	
	121	21	
	120.5	19	
	120	19	

TABLE 7

Reflected Intensity Data for the
(10) and ($1\bar{1}$) Level Splitting

7/6/76	(00) Beam	Sample Cooled to 85°K
	Sample Angle (deg)	Intensity (mv)
ϕ = 13°	108	0.095
	107	0.052
	106	0.11
	106.5	0.054
	107.5	0.080
	105	0.16
	104	0.27
	103	0.062
	102	0.044
	101	0.074
	101.5	0.061
ϕ = 12°	108	0.11
	107	0.091
	106	0.050
	105	0.13
	105.5	0.10
	106.5	0.055
	104	0.21
	103	0.16
	102	0.062
	101	0.072
	100	0.075
	102.5	0.060
ϕ = 10°	110	0.17
	109	0.16
	108	0.16
	107	0.17
	106	0.22
	105	0.25
	104	0.34
	104.5	0.29
	105.5	0.30
	103	0.59
	102	0.19
	101	0.10

TABLE 7 (Continued)

7/6/76	(00) Beam	Sample Cooled to 85°K
	Sample Angle (deg)	Intensity (mv)
ϕ = 10°	100	0.11
	99	0.12
	98	0.19
	100.5	0.10
	100.75	0.10
ϕ = 8°	107	0.14
	106	0.22
	105	0.13
	104	0.11
	103	0.15
	103.5	0.12
	104.5	0.10
	104.25	0.10
	102	0.29
	101	0.075
	100	0.067
	99	0.070
	98	0.070
	99.5	0.066
ϕ = 6°	110	0.064
	109	0.089
	108	0.13
	107	0.12
	106	0.13
	105	0.12
	104	0.035
	103	0.050
	104.5	0.040
	103.5	0.043
	102	0.072
	101	0.090
	100	0.053
	99	0.062
	98	0.038
	97	0.13
	97.5	0.075
	98.5	0.060

TABLE 7 (Continued)

7/6/76	(00) Beam	Sample Cooled to 85°K
	Sample Angle (deg)	Intensity (mv)
ϕ = 4°	110	0.14
	109	0.11
	108	0.087
	107	0.080
	106	0.096
	105	0.13
	104	0.035
	103	0.040
	102	0.049
	103.5	0.036
	104.5	0.053
	101	0.091
	100	0.082
	99	0.056
	98	0.064
	97	0.13
	98.5	0.047
	99.5	0.068

BIBLIOGRAPHY

1. J. A. Meyers and D. R. Frankl, Surf. Sci., 51, 61 (1975).

2. R. Frish and O. Stern, Z. Physik, 84, 430 (1933).

3. J. E. Lennard-Jones and A. F. Devonshire, Nature, 137, 1069 (1936).

   A. F. Devonshire, Proc. Roy. Soc. (London), A156, 37 (1936).

4. J. Anderson, "Molecular Beams from Nozzle Sources," in Molecular Beams and Low Density Gas Dynamics (Dekker, New York, 1974), P. O. Wegener, ed., 1.

   J. Anderson, R. P. Andres, and J. B. Fehn, Advances in Chemical Physics, Vol. 10, (Intersciences, New York, 1966), J. Ross, ed., 275.

   A. Kantrowitz and J. Grey, Rev. Sci. Instr., 22, 328 (1951).

5. D. R. Frankl, Rev. Sci. Instr., 45, 1375 (1974).

6. J. A. Meyers, Ph.D. Thesis, The Pennsylvania State University, 1975.

7. W. H. Weinberg, Adv. in Colloid and Interface Sci., 4, 301 (1975).

   J. P. Toennies, Appl. Phys., 3, 91 (1974).

   W. A. Steele, The International Encyclopedia of Physical Chemistry and Chemical Physics, Vol. 14, The Interaction of Gases with Solid Surfaces (Pergamon Press, New York, 1974).

8. H. Wilsch, H. U. Finzel, H. Frank, H. Hoinkers, and H. Nahr, Japan. J. Appl. Phys. Suppl. 2, Pt. 2 (1974).

9. B. Wood, B. F. Mason, and B. R. Williams, J. Chem. Phys., 61, 1435 (1974).

10. A. Tsuchida, Surf. Sci., 14, 375 (1969).

11. J. R. Bledsoe, Ph.D. Thesis, The University of Virginia, 1972.

12. N. Cabrera, V. Celli, F. O. Goodman, and R. Manson, Surf. Sci., 19, 67 (1970).

13. G. Wolken, Jr., J. Chem. Phys., 58, 3047 (1973).

14. H. Chow and E. D. Thompson, Surf. Sci., 54, 269 (1976).

15. R. J. Leroy, Preprint, 1976.

16. D. E. Houston, Ph.D. Thesis, The Pennsylvania State University, 1973.

17. H. Chow and E. D. Thompson, Preprint, 1976.

DISTRIBUTION

Commander (NSEA 09G32)
Naval Sea Systems Command
Department of the Navy
Washington, D.C. 20362 — Copies 1 and 2

Commander (NSEA 0342)
Naval Sea Systems Command
Department of the Navy
Washington, D.C. 20362 — Copies 3 and 4

Defense Documentation Center
5010 Duke Street
Cameron Station
Alexandria, VA 22314 — Copies 5 through 16